# Examination of gully sites on Mars with the shallow radar

Daniel Cahn Nunes,[1] Suzanne E. Smrekar,[2] Ali Safaeinili,[2,3] John Holt,[4]
Roger J. Phillips,[5] Roberto Seu,[6] and Bruce Campbell[7]

Received 17 September 2009; revised 21 January 2010; accepted 22 February 2010; published 12 October 2010.

[1] Martian gullies, found on steep slopes along broad mid-latitudinal bands, have morphologies resembling those of water-carved gullies on Earth and have been dated to <10 Ma. As such, one of the leading hypotheses, though not unique, is that martian gullies formed by the flow of liquid water in the very recent geologic past. Since the permittivity of liquid water is about one order of magnitude higher than that of most silicates, it is plausible that subsurface geologic interfaces involving liquid water may be detected via ground penetrating radar. We have surveyed a substantive portion of the martian gully population with data from the Shallow Radar (SHARAD) instrument, on board the Mars Reconnaissance Orbiter (MRO), in search of strong subsurface radar reflections indicative of the presence of liquid water reservoirs, which would serve as sources to the flows occurring within gullies. No such reflections are found at most of the locations surveyed, suggesting that either liquid water is not likely present in detectable amounts or that the shallow martian subsurface is unusually electrically conductive (i.e., lossy) at all of the locations examined. Strong subsurface reflections occur in the vicinity of gullies at two locations in the northern lowlands: Arcadia and southeastern Utopia Planitiae. In both cases, the reflectors occur at a range in depth of 45 to 90 m, considering a range in permittivity of 3 to 10, and −20 to −30 dB weaker than the surface reflection. In the case or Arcadia, the reflector corresponds to the eastern edge of Plaut et al.'s (2009) extensive radar subsurface unit; in both Arcadia and Utopia we interpret the reflectors as ground ice. Though our results offer a general assessment of the gully population, SHARAD is continuing its survey of gully rich locations.

**Citation:** Nunes, D. C., S. E. Smrekar, A. Safaeinili, J. Holt, R. J. Phillips, R. Seu, and B. Campbell (2010), Examination of gully sites on Mars with the shallow radar, *J. Geophys. Res.*, *115*, E10004, doi:10.1029/2009JE003509.

## 1. Introduction

[2] The observation of outflow channels and valley networks offered some of the first evidence for abundant fluvial activity early in the history of Mars [*Carr*, 1979; *Carr and Clow*, 1981; *Sharp and Malin*, 1975]), but the fate of that water has been a topic of intense investigation for the past twelve years. Recent data have shown water ice to be present at the martian surface and shallow subsurface at greater quantities then previously known. Infrared remote sensing by the OMEGA instrument (Observatoire pour la Mineralogie, l'Eau, les Glaces et al Activité, aboard Mars Express, MEx) confirmed that the perennial ice caps are composed of water ice [*Bibring et al.*, 2004], while radar sounding by the MARSIS (Mars Advanced Radar for Subsurface Ionosphere Sounding, aboard MEx) and SHARAD (Shallow Radar, aboard Mars Reconnaissance Orbiter, MRO) instruments showed the bulk of the polar layered deposits to be consistent with nearly pure water ice [*Picardi et al.*, 2005, *Phillips et al.*, 2008, respectively]. Gamma ray and neutron spectrometry (GRS instrument aboard Mars Odyssey) detected abundant hydrogen in the first meter of the near polar regolith, equivalent to ~35% of ice by weight [*Boynton et al.*, 2002; *Feldman et al.*, 2002]. The Phoenix lander, in turn, verified the presence of ground ice within ~10 cm of the surface at 68°N [*Smith et al.*, 2009], as predicted by thermodynamical models [*Mellon et al.*, 2008]. Evidence for surface water ice throughout the mid-latitudes is also mounting. SHARAD data show that the volume of the lobate debris aprons (LDA), which bear morphological similarities to glaciers but consist of silicate material at their surface, is consistent with massive ice [*Holt et al.*, 2008; *Plaut et al.*, 2009b].

[3] Support for the occurrence of liquid water in the martian past has also grown. The OMEGA and CRISM

[1]Jet Propulsion Laboratory, California Institute of Technology, Pasadena, California, USA.
[2]Earth and Space Science, Jet Propulsion Laboratory, California Institute of Technology, Pasadena, California.
[3]Deceased 29 July 2009.
[4]Department of Geological Sciences, University of Texas at Austin, Austin, Texas.
[5]Planetary Sciences, Southwest Research Institute, Boulder, Colorado.
[6]Dipartimento INFOCOM, Università di Roma "La Sapienza," Rome, Italy.
[7]Center for Earth and Planetary Studies, Smithsonian Institution, Washington, DC, USA.


0148-0227/10/2009JE003509

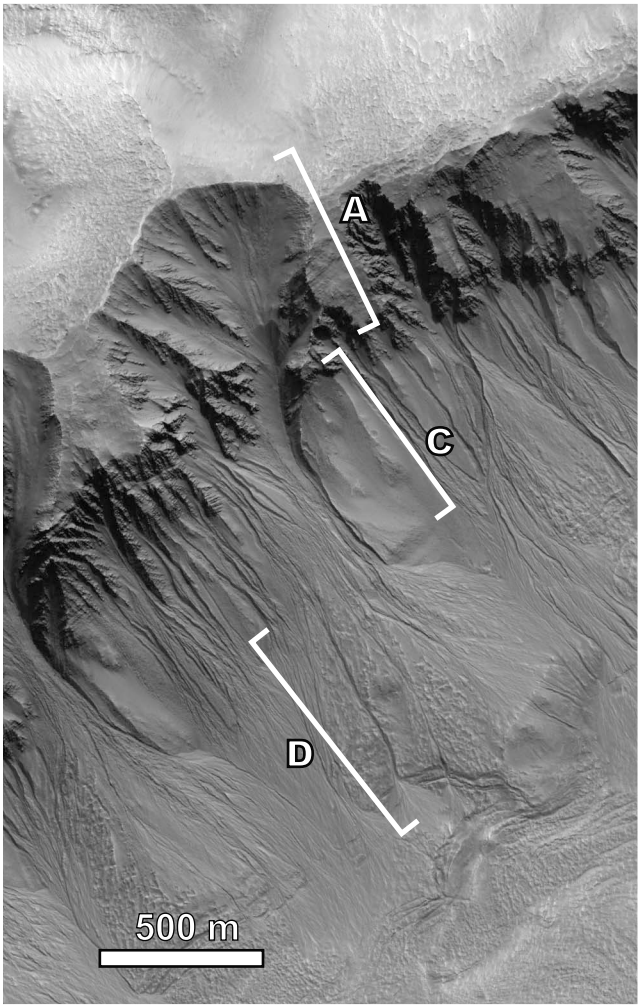


**Figure 1.** Example of a stereotypical gully containing an alcove (A), channels (C), and a debris apron (D). Cropped from HiRISE image PSP003675_1375 of a gully rich section of Newton crater (42.3°S, 201.8°E, approximately).

(Compact Reconnaissance Imaging Spectrometers, aboard MRO) spectrometers have detected the presence of sulfates and phyllosilicates, $H_2O$ or OH- bearing minerals generally formed by aqueous alteration of magmatic rocks or by evaporitic deposition [*Mustard et al.*, 2008; *Poulet et al.*, 2005]. The occurrence of these minerals on Mars, as seen by the orbital spectrometers, is spatially limited and stratigraphically linked to the Noachian epoch, when the planet was warmer and liquid water was likely stable at the surface. The rover Opportunity discovered at Meridiani Planum sulfate-bearing sedimentary bedrock that was likely formed by inundation and percolation of shallow surface water during the Noachian [*Squyres et al.*, 2006]. Aqueous alteration also transpired deep within the crust, as supported by the presence of phyllosilicates in crater ejecta and central peaks [*Mustard et al.*, 2008]. Indeed, aquifers have been hypothesized for Mars [e.g., *Clifford*, 1987; *Clifford and Parker*, 2001; *Hanna and Phillips*, 2005], but models generally focused on explaining groundwater activity during the wetter Noachian and Hesperian epochs of early Mars' history.

[4] The best evidence for geologically recent or even current fluid water action arises in the form of gullies, first discovered in Mars Orbiter Camera (MOC, aboard Mars Global Surveyor) images by *Malin and Edgett* [2000]. These features are similar in morphology to water-carved gullies on Earth, generally with an alcove-channel-apron morphology (Figure 1). They occur on steep slopes predominantly at the intermediate latitudes of both Martian northern and southern hemispheres. After the initial analysis indicating a polar-facing slope preference for their occurrence [*Malin and Edgett*, 2000], careful examination of the gully population has indicated that gullies do not tend to have a fixed preferred orientation, but rather that orientation varies slightly from region to region, as shown by *Heldmann and Mellon* [2004] and *Heldmann et al.* [2007]. Other analyses also documented orientation variation as a function of latitude, with pole-facing orientation dominating the gully population at mid-latitude and multiple orientations occurring at higher latitudes [e.g., *Balme et al.*, 2006 and *Dickson and Head*, 2009]. *Balme et al.* [2006], however, determined that a non-negligible (10 to 20%) fraction of gullies in the southern hemisphere occur on the slopes of isolated knobs and hills, a situation that is more difficult to reconcile with an aquifer source for liquid water. *Dickson and Head* [2009] noted that in these cases, gully morphology and orientation are indistinguishable from those of gullies on non-isolated slopes, suggesting, perhaps, a surficial instead of a subsurface control on gully morphology.

[5] While *Malin and Edgett* [2000, 2001] observed that, regionally, gullies originate from slopes at approximately constant depths of a few hundred meters, usually from an outcropping competent layer [*Malin and Edgett*, 2000; 2001], there is substantial variation in the morphology and geologic setting of gullies to complicate any effort in providing a single and simple explanation to their origin [*Treiman*, 2003]. For example, using imagery from the High Resolution Imaging Science Experiment (HiRISE), *Dickson and Head* [2009] showed that in addition to a main channel emanating from their bottoms, alcoves also possess smaller channels throughout their domain, which converge and coalesce into the main channel. Such a finding alleviates the necessity of having a single layer as the possible (local) source of ground water.

[6] Notably, *Malin et al.* [2006] observed the emplacement of bright digitate deposits emanating from the channels of a few select gullies. These deposits appear to derive from low viscosity flows, as they conform to minor topographic obstructions and have no detectable thickness within the resolution of MOC (~3 m/pix). This finding elevates the possibility of current fluid activity, albeit minor, on the martian surface. Observations with HiRISE at ~0.3 m/pix confirm the relationship between bright deposits and gully channels and show that the channels appear otherwise unmodified by these flows [*McEwen et al.*, 2007]. The fact that the bright deposits persist over the 15 months between MOC and HiRISE observations suggests that the elevated brightness of these deposits is not due to frost or ice [*McEwen et al.*, 2007]. Dust, which is generally brighter than sand and rocks on Mars, could also explain the brightening and would not necessarily indicate the action of water. Analysis of near-infrared data from CRISM does not indicate the presence of hydrated minerals in the bright

deposits, as it would be expected from evaporation of salty groundwater [*McEwen et al.*, 2007]. Conversely, the analyses of high-resolution (meter scale) digital elevation models (DEM's) produced form HiRISE stereopairs show that deposition begins to occur at slopes shallower than it would be otherwise expected for dry granular flow, the implication being that some sort of fluidizing agent was involved in these flows [*Kolb et al.*, 2009]. The stratigraphic investigation of *Schon et al.* [2009], linking secondary craters on the apron deposits of a gully to a primary crater dated to ~1.25 Ma, places a constraint on flow ages and suggests a link to orbitally forced climate variations as the driving force to activity. And so, even with greater amounts of data and improvements in resolution, the mechanism behind gully formation has not yet been positively identified.

[7] The formation models involving the action of fluids fall into two broad classes. One is the production and transport of fluids (generally water) in distinct geologic layers at depth to an eventual outburst or seepage at steep slopes [e.g., *Mellon and Phillips*, 2001]. The other class entails fluid production in surficial deposits, such as a snowpack [e.g., *Christensen*, 2003]. Finally, there is a third class of gully formation models that involve dry mass wasting of some sort [e.g., *Treiman*, 2003]. Because the dielectric permittivities of liquid water and brines are much higher than those for rock forming silicates and the expected depth for the source of the liquid water forming gullies is a few hundred meters, SHARAD is a valuable asset to further investigate the hypotheses of gully formation involving water or brines. Here we focus on the search for possible subsurface reflectors consistent with a shallow aquifer in the SHARAD data. We present the first set from our campaign of gully observations; although the coverage of the gully population is only partial, some first order conclusions are possible. Later we present the results from modeling the propagation of SHARAD signal through the subsurface to provide context to our data interpretation.

## 2. SHARAD Basics

[8] SHARAD, provided by the Agenzia Spaziale Italiana (ASI) as an instrument on MRO, is a chirped nadir-looking radar sounder (Table 1) that offers the capability of probing hundreds of meters into the shallow subsurface at an approximate vertical resolution of 10 meters for the more common silicic geologic materials [*Seu et al.*, 2007]. Such penetration ability and vertical resolution are compatible with the expected depth and thickness of putative aquifers as based on observations of gully occurrence and hydrologic models [*Malin and Edgett*, 2000; *Mellon and Phillips*, 2001]. In contrast, the lateral resolution of SHARAD is limited to 300 m along-track and 3 km cross-track, which is too coarse to allow individual gullies to be observed. Consequently, our approach relies on the identification of subsurface reflectors in gully rich areas that have compatible depths and that can perhaps be traced all the way to slopes hosting gullies. Radar reflectors arise from a contrast in dielectric permittivity ($\varepsilon$) across an interface between two media, such as that between the atmosphere and the crust or that between two successive geologic units. Composition and porosity are typical drivers of variations in $\varepsilon$. Due to the much higher permittivity of water ($\varepsilon_{water} \sim 80$ for near freezing temperatures and SHARAD frequencies [*Ulaby et al.*, 1986]) with respect to common crustal rocks ($4 < \varepsilon_{rock} < 10$ [*Ulaby et al.*, 1986]), the presence of water in the pore space of a distinct geologic layer has the potential of producing a strong subsurface radar reflection.

[9] There are two complicating factors inherent to the radar sounding technique that affect our study. One is surface clutter, where reflections from off-nadir surface topography arrive at the spacecraft after the surface reflection from nadir and may overprint or be erroneously identified as subsurface reflections [e.g., *Phillips et al.*, 1973; *Seu et al.*, 2004]. Clutter intensity is dependent on the relief of the targeted terrain and is generally more prominent at the heavily cratered Martian southern highlands than at the generally smoother northern lowlands. We identify clutter for specific radar observations by simulating surface reflections of the SHARAD pulse arising from the Mars Orbiting Laser Altimeter (MOLA) 128 pixel/degree digital elevation model (DEM). Because the clutter simulation is based on an ideal signal and lacks noise and other sources of signal degradation, it tends to show a more intricate clutter picture than the actual radargrams.

[10] The second complicating factor is the presence of sidelobes, which are a ringing-like sequence of successive weaker peaks that follow a reflection (the main lobe or peak) and arise from the pulse compression technique utilized by SHARAD to achieve the desired energy output and range resolution [e.g., *Seu et al.*, 2007]. To reduce sidelobe amplitudes produced by the surface reflection and avoid the masking of weak subsurface reflections, a weighting function (nominally a Hanning function for SHARAD) can be applied to the chirp signal. This suppression technique, however, broadens the reflection's main lobe and can cause a relatively strong and shallow reflection to be indistinguishable from the surface reflection. Choosing whether a case necessitates avoidance of sidelobe suppression is not always clear, and experimentation may be necessary depending on depth and strength of a given suspected reflector.

## 3. Observations

### 3.1. General (Locations, General Findings, Clutter, Sidelobes)

[11] We have examined 65 different locations within the two mid-latitudinal bands where gullies concentrate (Figure 2). These include locations where SHARAD observations were specifically targeted at gullies, where other SHARAD observations coincidentally sampled gullies, and areas in the northern plains between groups of gullies but not containing gullies themselves. As previously stated, our goal is not identifying individual gullies because they lie below the resolution of SHARAD. Instead, our goal is to hopefully detect the hypothesized aquifers feeding the fluid carving the gullies, if present, and determine their geographic extent. Although it includes only a fraction of all of the gully occurrences, the sampling shown in Figure 2 adequately supports such a goal. In their mapping, *Heldmann et al.* [2007] identified eastern Arcadia Planitia, Tempe Terra, Acidalia Planitia, and Utopia Planitia as locations where gullies concentrate in the northern hemisphere. In the southern hemisphere, *Heldmann and Mellon*

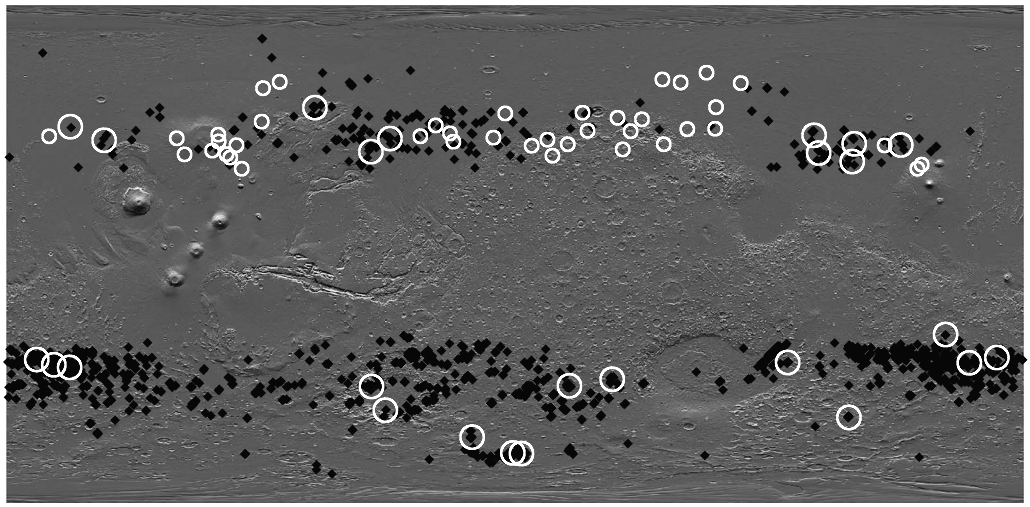

**Figure 2.** Shaded relief map of Mars based on the MOLA 128 pixel/degree cylindrical projection grid available through the Planetary Data System (PDS), showing locations containing gullies as mapped by *Heldmann and Mellon* [2004] and *Heldmann et al.* [2007] (black diamonds) and areas examined in this paper (white circles).

[2004] identified Dao Vallis, the south polar pits, and Terra Sirenum as the main concentrations of gullies. All of these locations are sampled in our observations.

[12] In the great majority of the cases examined, radargrams fail to show positively the presence of subsurface reflectors. One such example is the examined portion of Acidalia Planitia centered approximately at 41.7°N, 326.4°E that includes Hesperian-aged mottled, grooved, and ridged plains [*Skinner et al.*, 2006] and lies among craters containing gullies (Figure 3A). These craters containing gullies range in size from 5 to 40 km and their slopes tend to be composed of massive blocks with limited layering exposed at portions of their walls. Gullies occur on both massive and layered portions of the walls and tend to present elongate alcoves, channels, and limited debris aprons. Accompanying the DEM in Figure 3A are two radargrams in Figure 3B covering the inter-crater area (SHARAD product ID's 477101 and 590502); they show a slightly rough surface and small-scale (short-wavelength) clutter associated with knobs and ridges arriving before and after the main surface reflection. In some portions of these radargrams there are radar returns that appear to be subsurface reflections occurring within less than 2 $\mu$s of the surface; they are very limited laterally, are generally weaker than 30 dB with respect to the surface reflection, and are not constant in depth. Based on the clutter simulations, we interpret these secondary returns as clutter from small-scale surface topography, some of which is not necessarily resolved by MOLA.

[13] Another example in western Acidalia Planitia is the area around Gamboa crater (40.75°N, 315.63°E), an Amazonian-aged smooth plains unit [*Skinner et al.*, 2006] (Figure 4). Gullies in this area occur on the slopes of the larger craters (>10 km, including Gamboa) where layered outcrops are seen. Eleven radargrams cover the Gamboa crater area, and here we highlight two that transect the crater itself (417802 and 694702). Again, there are no obvious subsurface reflectors extending through the scene that could be interpreted as an aquifer (Figure 5. To the north (left on radargram) and south of the crater the surface reflections are well defined by a single peak, indicating a more specular characteristic and implying a smooth surface. The surface reflection becomes diffuse within 1 to 2 crater diameters around the crater, which corresponds to the Gamboa ejecta

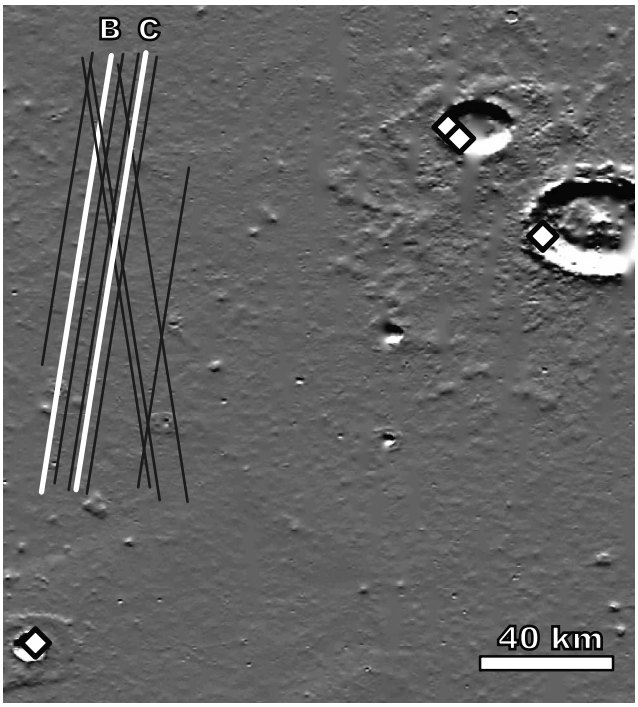


**Figure 3a.** MOLA DEM of a portion of Acidalia Planitia containing gullies (white diamonds); center is approximately 40.95N, 327.71E. Lines denote SHARAD tracks, of which those highlighted in white (B and C) correspond to the radargrams shown in Figure 3B.

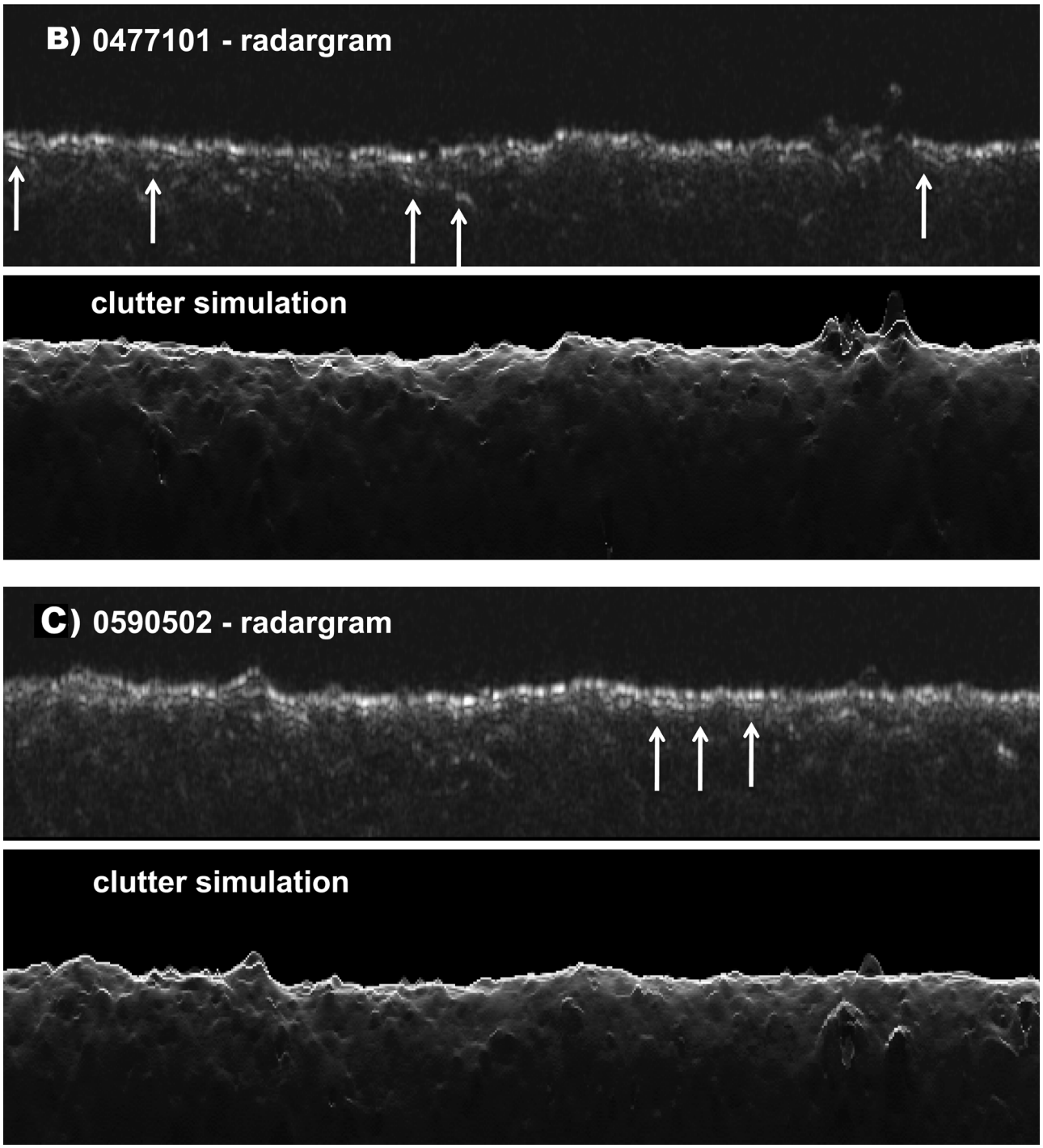


**Figure 3b.** Radargrams 477101 and 590502 are for the two SHARAD tracks highlighted in Figure 3A. White arrows denote small reflections occurring later than the local surface reflection that are likely produced by small-scale surface relief, as shown by the accompanying surface clutter simulations.

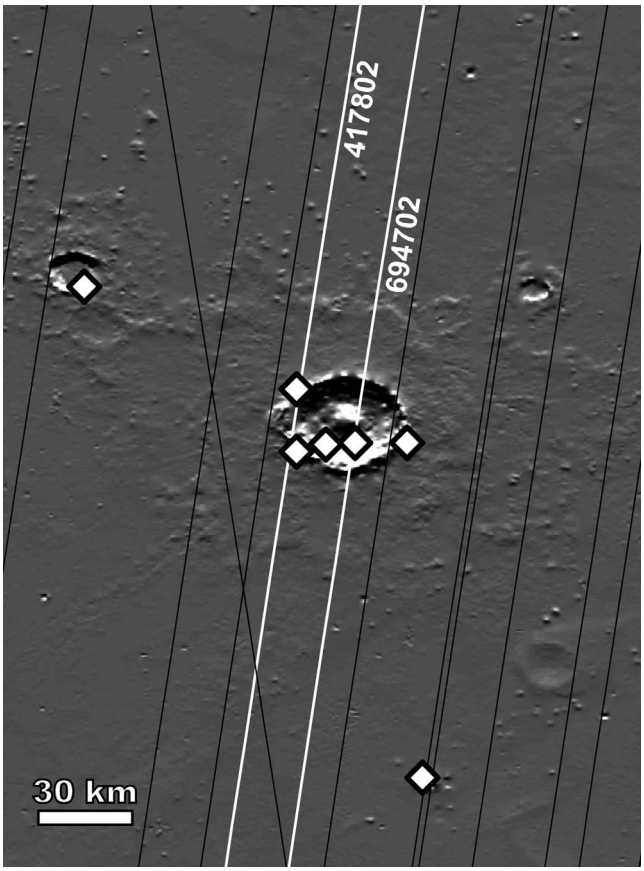


**Figure 4.** MOLA DEM centered on Gamboa crater (40.82°N, 315.67°E) in Western Acidalia Planitia (Amazonian smooth plains). Lines correspond to SHARAD tracks and white diamonds to gully locations. Highlighted tracks correspond to the radargrams shown in Figure 5.

blanket and indicates substantial surface scattering due to terrain roughness. Over the crater, the radargram surface reflection slopes upwards to reveal the elevated rim, and some clutter appears in response to the rim and the rough crater wall. A couple of weaker returns follow the surface reflection in the smooth plains area of the radargrams in Figure 5 (insets). The earlier (upper) of these two closely follow the surface reflection both in shape and power variations, vanishing beneath the area of the plains near the ejecta blanket. The lower of these returns, best seen in 694702, is found intermittently and is close to the noise level. Since sidelobes tend to be more prominent where surface reflections are strong and nearly specular, such as in this case, we applied different signal processing techniques (i.e., pulse weighting and focusing, as explained in *Seu et al.* [2007]). Though the strength of the shallowest of these returns changed depending on the processing scheme (Figure 6), which favors to a sidelobe interpretation, it was not entirely suppressed. Clutter simulation does not produce such a feature either, so it is possible that this weak and shallow return corresponds to a real subsurface dielectric interface at ~0.3 $\mu$s after and ~40 dB weaker than the surface reflection. Assuming a range in permittivity range between 4 and 9 for the regolith, this corresponds to a reflector depth between 30 and 45 m.

[14] Given that craters are one of the dominant settings for gullies, it is important to note that the characteristics of the data over Gamboa are pertinent to SHARAD data at other gully locations on Mars. The diffuse signature of an ejecta blanket make it more difficult or may even entirely mask the observation of a potential subsurface reflector all the way to the crater wall containing gullies, which would strongly link subsurface reflectors to gullies and inspire greater confidence in the aquifer hypothesis of gully formation (such observation has not been made thus far). This effect is illustrated in Figure 7, which displays the results from laterally averaging the radargram for each of three areas north of the crater in 694702 (Figure 5). The average power of the surface reflection from the smooth plains unit far from the crater is 44 dB (>60 dB at individual spots) and much higher than over the ejecta blanket, where it is severely depressed in power (~11 dB) and broadened in range with multiple peaks. More importantly, a slowly decaying tail follows the ejecta surface reflection (>13.5 $\mu$s) that is at least 2 to 5 dB higher than the noise level seen at the smooth plains and might swamp the signal from a weak shallow reflector. This elevated "noise" level is dependent on location and is higher for rougher surfaces.

[15] The Newton crater (40.5°S, 158.3°E, ~350 km in diameter) area contains one of the largest gully concentrations in the highlands and is a natural target of our observations. The crater, seen in Figure 8, lies in the Noachian-aged plateau cratered unit, and its extensive floor corresponds to Hesperian ridged plains unit [*Skinner et al.*, 2006]. It hosts numerous smaller superposed gully-bearing craters on its rim and floor [e.g., *Head et al.*, 2008], and gullies with different morphologies, orientations and elevations; this variety perhaps suggests a pervasive subsurface source for water. We focus on two radargrams that capture the general appearance of the abundant radar dataset at Newton. Figure 9 shows radargrams 990501 and 993801 on the eastern side of Newton that transect a smaller crater hosting gullies. Rim and wall topography of Newton produces substantial clutter at both northern (left) and southern ends of the radargrams. Ridges on the floor of Newton also produce clutter. Real subsurface reflectors would likely hold their respective positions to the surface between the upper and lower panels, while clutter slightly changes relative shape and position in the radargram because of the lateral shift from one track to the other. Only the latter is seen in the radargrams examined at Newton. The small crater containing the gullies is clearly seen near the midpoint of the floor. The reflection from the floor also possesses the near specular nature seen in the smooth units of the northern lowlands, including a weaker return (insets) following the surface that appear to be sidelobes in the same fashion to that seen in Figures 5 and 6. Throughout Newton and its smaller guest craters, we observe no subsurface reflectors in the multiple radargrams examined, which is in stark contrast to what would be expected if the abundant gullies were the surficial expression of ground water reservoirs.

### 3.2. Recently Active Gullies

[16] We have also examined a number of gullies that represent "best bets" for water detection based on the recency of their activity or on their geologic setting.

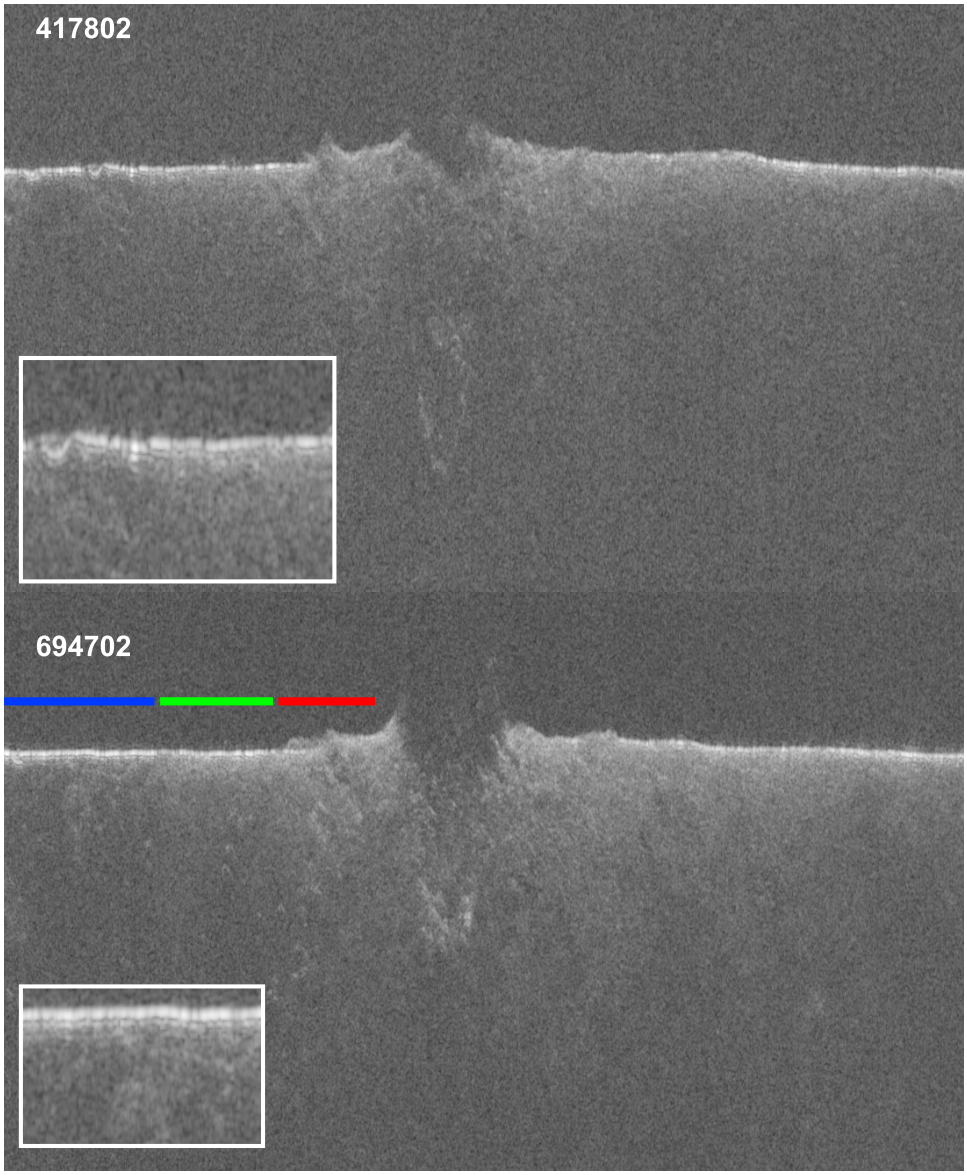


**Figure 5.** Sections of SHARAD radargrams 417802 and 694702 around Gamboa crater, highlighted in Figure 4. Insets correspond to the smooth plains on the northern (left) end of the tracks and show weak returns following the surface reflection. Color swaths added to 694702 correspond to sections in which the radargram has been averaged, as seen in Figure 7.

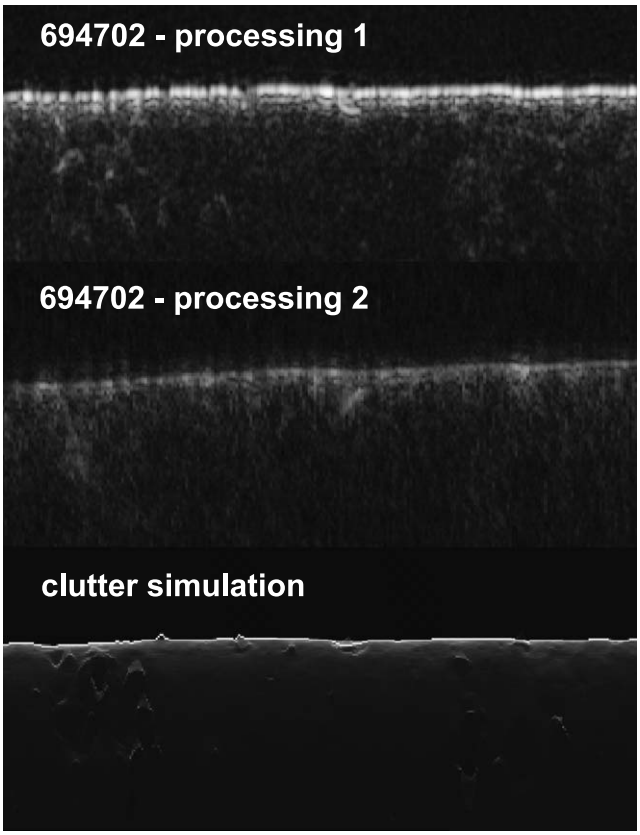


**Figure 6.** Different processing results for a portion of radargram 694702 showing the plains north of Gamboa and including the area of the insets in Figure 5. The shallow weak returns previously seen to follow the surface reflection over the smooth plains in Acidalia Planitia (top) are substantially reduced with different signal processing (middle) and do not appear in clutter the simulation (bottom).

[17] First we concentrate on gullies where activity is seen to be ongoing, as determined by the appearance of bright digitate flows within the past decade [*Malin et al.*, 2006]. If liquid ground water is feeding these flows, then there is a chance SHARAD may detect the putative aquifer source. The first location reported by *Malin et al.* [2006] is on the slopes of a 4-km crater in Terra Sirenum (Noachian plateau units, *Skinner et al.* [2006]), where there are several SHARAD tracks in the neighborhood and two directly targeted at the crater (788801 and 793401, Figure 10). These tracks also cover at their southern extremities two other craters containing gullies, but these show no indications of recent activity. The recent flow is bright and conforms to a gully channel, as shown by HiRISE (image PSP_004229_1435). The radargrams (Figure 11) distinctly show the valley floor and substantial clutter associated with the valley walls, craters, and other topographic features. An aquifer could appear as a consistent subsurface reflector at least near to the location of the crater (arrow) in both of the radargrams, but no such reflector is seen in either of the cases. The second location of current gully activity reported by [*Malin et al.*, 2006] is on the slopes of a 9-km crater in the Centauri Montes area at the head of Harmakhis Vallis (Hellas basin rim unit, Noachian in age [*Skinner et al.*, 2006]), in which other gullies have also been mapped. There is extensive SHARAD coverage in this area, including a track that goes right over the crater in question. The DEM in Figure 12 shows a very rough terrain at the northern (left) half of the track, which produces the heavy clutter seen in the radargram, Figure 13, and makes the identification of the crater extremely difficult. Again, no consistent subsurface reflector, as would be expected for an aquifer, is seen across the area.

[18] Another potentially interesting gully occurrence is on the south- (pole) facing wall of a 17-km crater centered at 28.9°S, 152.6°E (Figure 14 and arrows in Figure 14). This crater, located on a dissected plateau unit of Noachian age [*Skinner et al.*, 2006], has mostly smooth walls that have only slight indications of layering. A small NE–SW trending fault bisects this crater (Figure 15 and arrows in Figure 14), and it is at the intersection of this fault with the pole-facing wall that two gullies originate. Although a small crater is present on the slope where one of the gullies originates, we note that other similar small craters occur around the walls of the larger host crater but have no gullies. The observed gullies possess small alcoves, multiple channels of low sinuosity, and debris aprons that appear to superpose eolian deposits (dunes) on the crater floor. It is plausible that the small fault intersecting the crater could serve as a conduit for ground water to reach the surface if a deep aquifer were present. SHARAD targeted this location on two orbits, and one of these radargrams along with the simulated surface clutter is shown in Figure 16. A comparison between data and simulation show that the reflections occurring later than (or "below") the surface reflection are due to clutter, likely produced by the crater rim and wall, and by the relief associated with the fault. The diffuse appearance following the surface can be attributed to either surface roughness below the scale of MOLA or volume scattering within the subsurface. Nonetheless, there are no consistent subsurface reflectors across this region that could be attributed to an aquifer.

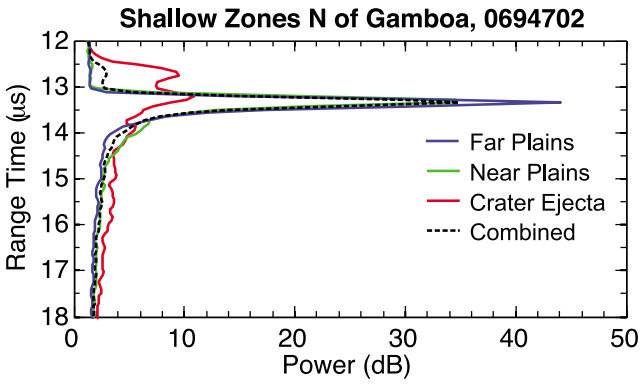


**Figure 7.** Averaged sections of the 694702 radargram to the north of Gamboa crater. Colors of curves correspond to the areal swaths marked in Figure 5, while the black dashed curve corresponds to the average radargram of the three areas combined.

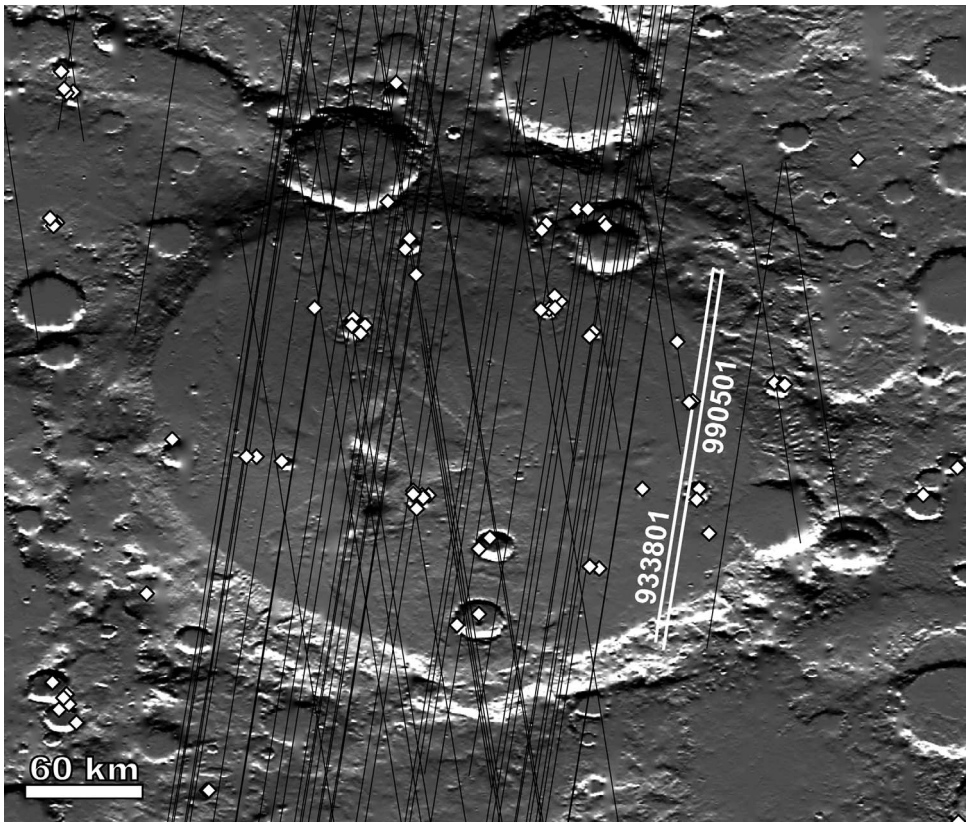


**Figure 8.** MOLA DEM of Newton crater (40.5°S, 158.3°E) and portions of the surrounding southern highlands (Noachian plateau sequence, cratered unit). Lines correspond to SHARAD tracks and white diamonds to gully locations. Radargrams for the highlighted tracks are shown in Figure 9.

### 3.3. Promising Sites (Arcadia and Utopia Planitiae)

[19] Of the sites we have examined, seen in Figure 2, two show substantial subsurface reflectors near gully occurrences. The first site is in southeastern Arcadia Planitia (40.8°N, 215.2°E), where a limited number of craters in the Amazonian-aged Arcadia Formation members [*Skinner et al.*, 2006] possess gullies on their walls (Figure 17). Some of these gullies appear to originate at distinct layers (or even overhangs) on the wall of a host crater, while others are nested on massive blocks or mantled surfaces on other crater walls. The entire region is covered with SHARAD tracks and was analyzed by *Plaut et al.* [2009a], who mapped a radar subsurface unit that spans from 180°E to 225°E. The initial assessment of *Plaut et al.* [2009a], based on a range of permittivity from 3 (pure water ice or low-density sediments) to 8 (basalt), is that the reflector lies at a depth between 50 and 90 m and that the radar signal is not strongly attenuated by the overburden. These characteristics and the presence of geomorphic indicators of subsurface ice led *Plaut et al.* [2009a] to favor the (non-unique) interpretation of ground ice for this extensive reflector. Although the area of this reflector encompasses many craters, few contain gullies as mapped by *Heldmann and Mellon* [2004] and *Heldmann et al.* [2007]. Those containing gullies are adjacent to the eastern side of *Plaut et al.*'s [2009] mapped unit (Figure 17). We analyzed a number of radargrams in this area, of which we highlight two, 704302 and 783401; portions of interest from these radargrams are shown in Figure 18. In both cases a strong subsurface reflector occurs between two of the craters possessing gullies. The depth of this reflector ranges between 0.55 $\mu$s to 0.85 $\mu$s. Its reflected power varies between −15dB to −30 dB with respect to the surface reflection and lies at ~10 dB above the noise level. In the two cases illustrated, the northern (left) extremity of the subsurface reflector is difficult to identify, as it appears to merge with the surface reflection. In contrast, the southern (right) extremity occurs abruptly at the ejecta blankets of craters containing the gullies; either the rough ejecta blankets scatters the surface reflection and masks the subsurface returns, as discussed previously, or the reflector indeed stops at the edge of the craters. This subsurface reflector we observe is continuous, although irregular in shape and power in the area of the DEM's seen in Figure 18, and it is likely the same reflector in *Plaut et al.* [2009]. If a genetic relationship exists between this reflector, which is attributed to ice, and the mapped gullies, it is difficult to ascertain, at this stage, beyond the apparent geographical co-location, as many other crater pockmark the radar unit but do not retain evidence for gullies.

[20] The second site that is dense with gullies and where we identify a strong subsurface reflector is southeastern Utopia Planitia. Figure 19 shows this area according to MOLA roughness on the scale of the DEM (~450 m/pixel) along with the locations of mapped gullies and the portions of SHARAD tracks where subsurface reflectors are seen. This area is peppered with craters containing gullies and

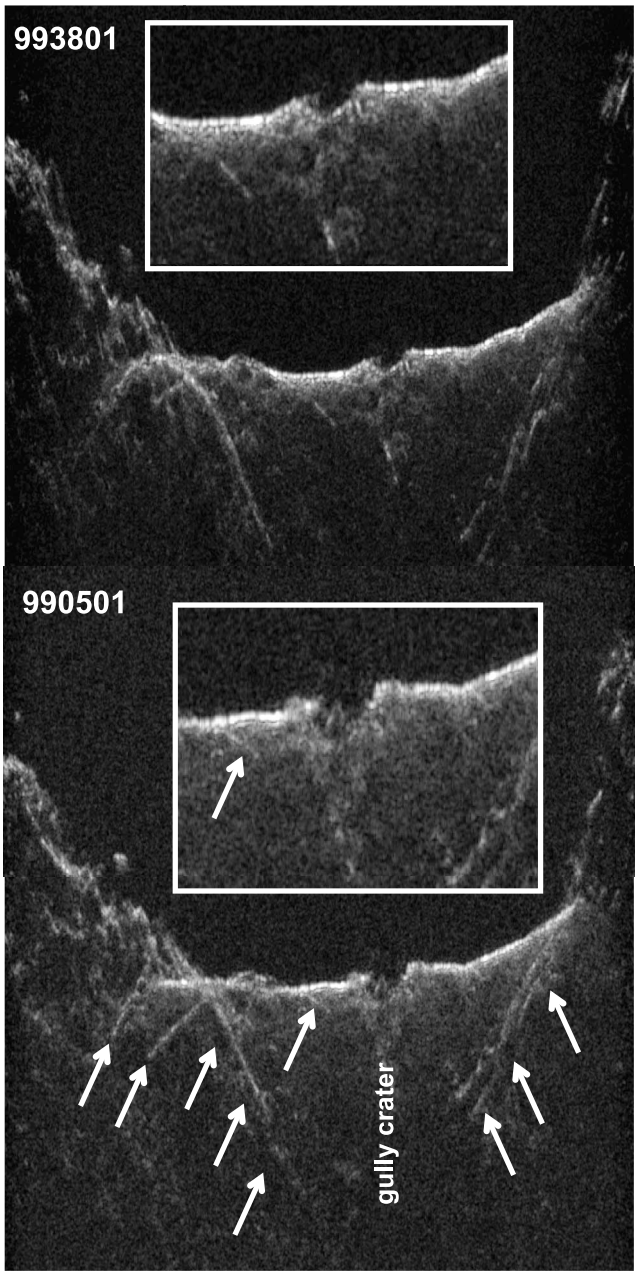


**Figure 9.** Two radargrams from Newton Crater corresponding to the highlighted SHARAD tracks in Figure 8 (990501 and 993801). White arrows point to clutter features in 990501 that arrive after the surface reflection; these same features appear in 993801 only slightly shifted in position and shape due to SHARAD track offset. The smaller crater containing gullies is seen at approximately the midpoint on the floor of Newton, and only sidelobes to the surface reflection are seen near this crater.

corresponds to Amazonian-aged Elysium Formation units and smooth plains units. Gullies appear from layered, massive, and mantled crater walls. This area is uniformly covered with SHARAD observations, and we highlight two tracks that intersect craters hosting gullies. On track 725701, seen in Figure 20, a subsurface reflector is present near the southern (right) end of the radargram, and is delineated by vertical white lines. This reflector lies < 1 $\mu$s after the surface reflection, is discontinuous, and correlates with the smoother surface units, as shown in Figure 19. At the northern end of the track, which abuts the ejecta blanket of a gully-bearing crater, the surface is rougher as seen by MOLA and no subsurface reflector is observed. Simulation of surface clutter does not show the reflector and confirms its subsurface nature (Figure 20). On 1221501, Figure 21, which lies ~10 degrees to the west from 725701, a subsurface reflector is seen on the southern end of the track. Again, the reflector is present where the surface is smooth as seen by MOLA, but it does not extend for the entirety of the smooth unit. Instead, its abrupt end to the north does not appear to correlate with relief features. Again, the reflector lies within ~1 $\mu$s of and is nearly parallel to the surface. Although similar in depth and appearance, the reflectors in 725701 and 1221501 are separated by 7° in latitude and 11°

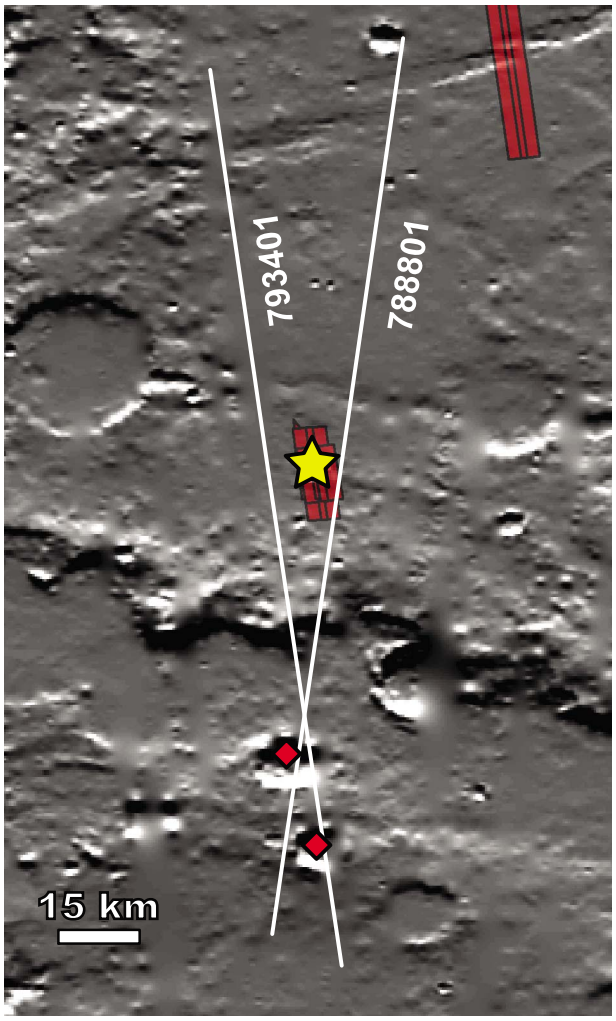


**Figure 10.** MOLA DEM centered at a small crater containing an active gully (yellow star) in Terra Sirenum (36.23°S, 198.27°E). The crater lies between the two SHARAD tracks (788801 and 793401) and beneath the red rectangle that outlines the footprint of HiRISE image PSP_004229_1435, which shows the recent bright flows of the active gully. Other gullies (diamonds) are seen at the southern (lower) end of the valley to the south of this crater.

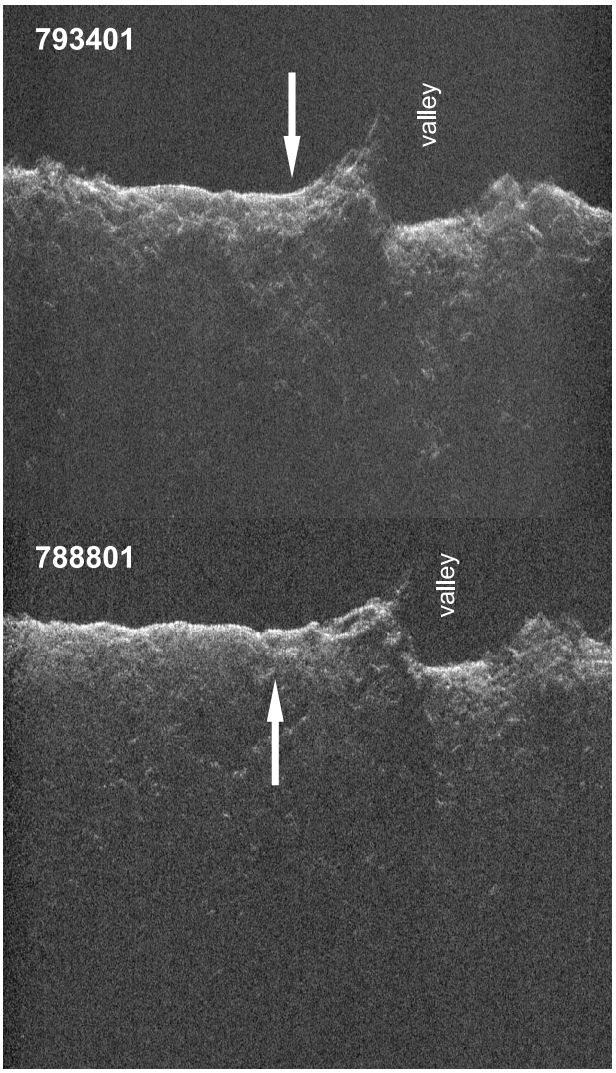


**Figure 11.** Radargrams for the two SHARAD tracks adjacent to the active gully marked in Figure 10. White arrows denote the location of the small crater hosting the gully. The valley to the south of this crater is defined by a strong reflection from its relatively smooth floor. Absent from these radargrams is a consistent subsurface reflector.

in longitude, giving us the suggestion that this radar unit may be somewhat extensive; we are currently mapping it.

## 4. Propagation Model

[21] The general absence of subsurface reflectors in association with gullies does not definitively preclude the existence of aquifers. Starting from the assumption that they exist, it is plausible that *i*) aquifers presently contain little water and produce only weak reflections that lie below the detection threshold of SHARAD, *ii*) aquifers contain enough water to produce strong reflections that are, in turn, attenuated by the overburden, or *iii*) aquifers contain substantial water but the geometry of their upper boundary are not conducive to producing strong reflections (i.e., not sharp or not smooth). In order to better characterize these scenarios and give context to the radar sounding observations, it is necessary to simulate the propagation of the SHARAD signal through a simple stratigraphic model and explore the parameter space defined by the water fraction and depth of an aquifer as well as the attenuating properties of the overburden. The main goal of this exercise is to place bounds on the amount of water necessary to produce an observable reflection and on the attenuation of such a reflection within the overburden.

[22] The modeling approach [*Nunes and Phillips*, 2006; *Ulaby et al.*, 1986] incorporates pulse compression of the simulated radar signal [e.g., *Ducoff and Tietjen*, 2008] with the one-dimensional propagation of plane waves through layered media [*Wait*, 1970]. This analytical approach has proved itself to be robust, as it successfully predicted the penetration of SHARAD signals to the base of the polar layered deposits (PLD) in places and the detection of internal PLD layering [e.g., *Phillips et al.*, 2008]. Note that

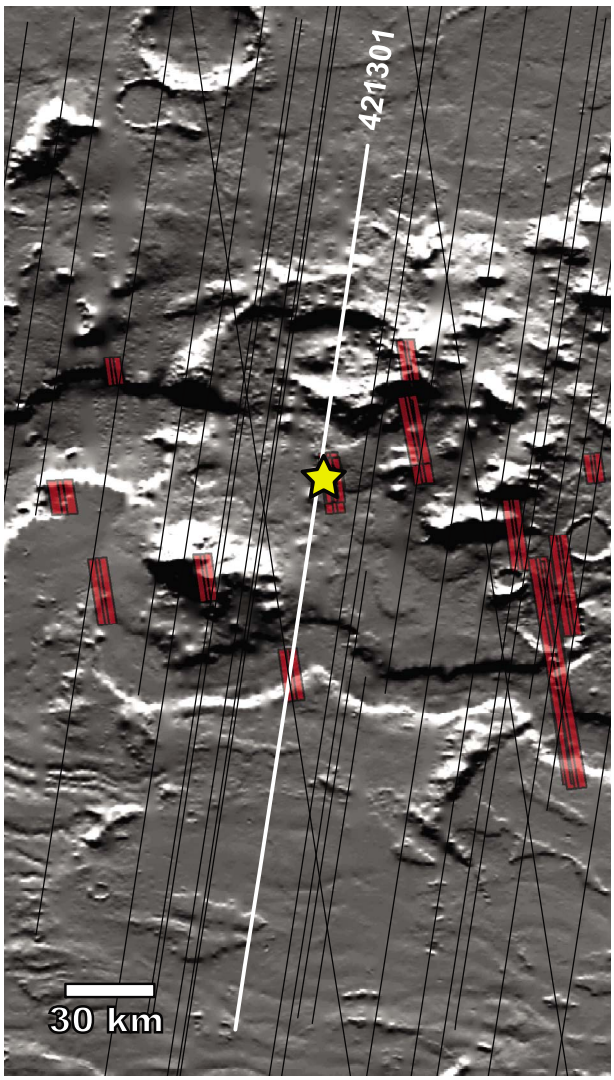


**Figure 12.** MOLA DEM centered at a small crater in Centauri Montes (38.38°S, 96.78°E) where an active gully is located (yellow star). SHARAD has covered this area substantially (black lines), with track 421301 transecting the targeted crater highlighted in white. Red rectangles represent HiRISE footprints.

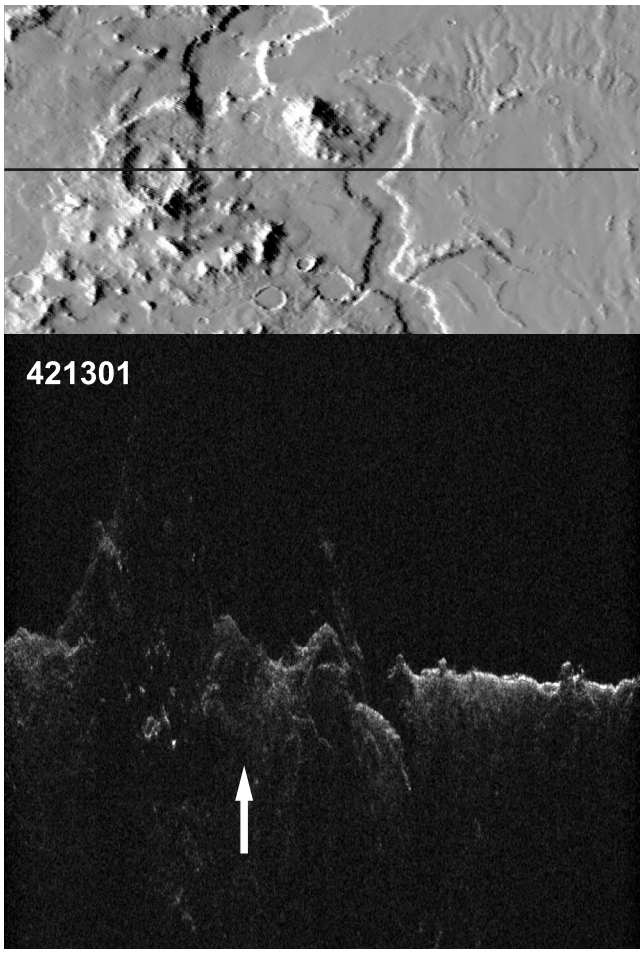


**Figure 13.** Radargram for track 421301, highlighted in Figure 12. Clutter dominates the northern (left) half due to very rough topography. No consistent subsurface reflector is observed throughout this scene.

this method only takes into account the complex electric permittivity when computing signal losses, which is appropriate for a number of target compositions that have low or negligible measured magnetic permeabilities (e.g., water ice, sand, ferric oxides, olivine, and maghemite [*Stillman and Olhoeft*, 2008]). For cases where magnetic losses are expected to be significant (as in soils bearing magnetite [*Stillman and Olhoeft*, 2008] and brines [*Ulaby et al.*, 1986]), our simulations represent a lower bound scenario. Note also that this method assumes smooth interfaces only, so losses due to scattering at a rough interface are not factored.

[23] The simplest stratigraphic model that can be applied in this study is that of two layers, the surface (or overburden) layer and the aquifer, overlying a crustal halfspace; this can represent the case where melting occurs within an ice-rich permafrost [*Costard et al.*, 2002]. A slightly more complex stratigraphic model is that of a confined aquifer, where an impermeable layer between the surface layer and the aquifer allows ground water to be pressurized [e.g., *Mellon and Phillips*, 2001; *Malin and Edgett*, 2000].

[24] The complex permittivity ($\varepsilon = \varepsilon' + i\varepsilon''$, relative to the permittivity of free-space) of each of the different elements of the stratigraphic model is not well constrained and the range of possible values is ample. The real portion ($\varepsilon'$) controls the reflection coefficient at interfaces and usually falls between 4.9 and 9.6 for bulk, dry volcanic materials according to composition [*Ulaby et al.*, 1986]. Measurements of the JSC Mars-1 Regolith Simulant (JSCM1 [*Allen et al.*, 1997]) at a density of 1.6 g cm$^{-3}$ yields $\varepsilon' = 2.84$ [*Stillman and Olhoeft*, 2008]. Adopting a mean crustal density of 3.3 g cm$^{-3}$ and applying the empirical density relationship of *Olhoeft and Strangway* [1975] yields $\varepsilon' = 8.61$, which falls within the range given by *Ulaby et al.* [1986]. Consequently, we adopt two different values for the effective real permittivity of the overburden layer: $\varepsilon'_{ov} = 5$ and 10. Obviously, this is a simple approximation to what should be in reality an increasingly denser regolith over depth, but it should suffice for placing bounds on the problem of propagation of radar waves through the overburden. We also adopt the same values for the permittivity of rock, $\varepsilon'_{rx} = 5$ and 10.

[25] The imaginary portion ($\varepsilon''$) controls signal attenuation along with radar frequency. *Olhoeft and Strangway* [1975] found it to vary by ~3 orders of magnitude in lunar compositions according mostly to FeO+$TiO_2$ content and density. Recent laboratory measurements by *Stillman and Olhoeft*

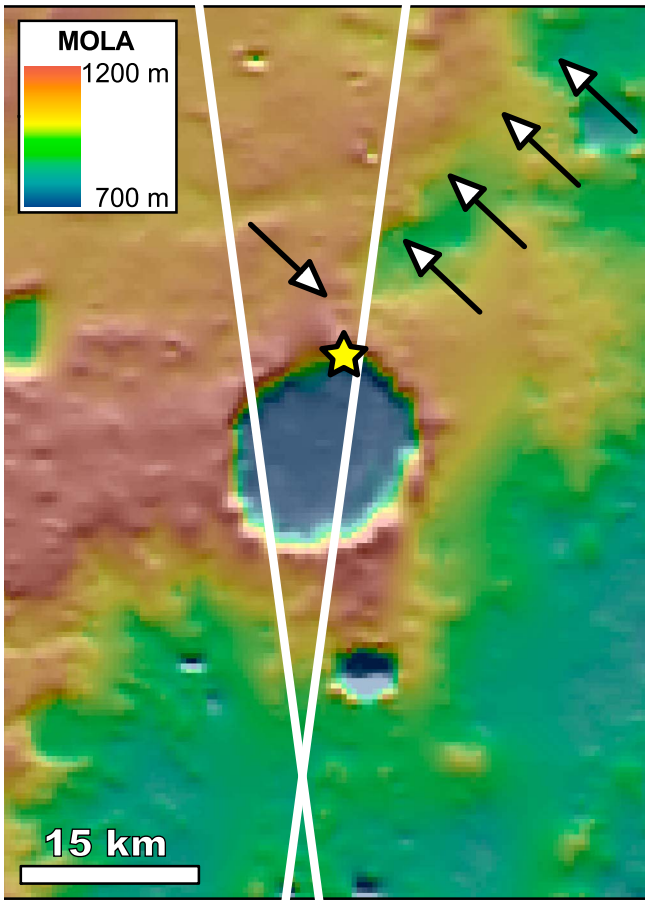


**Figure 14.** MOLA DEM centered at a small crater in Terra Cimmeria (28.93°S, 152.60°E) where gullies (yellow star) arise from the intersection between a fault (arrows) and the crater wall. Shown are the two SHARAD tracks that transect the crater (796201 and 798201).

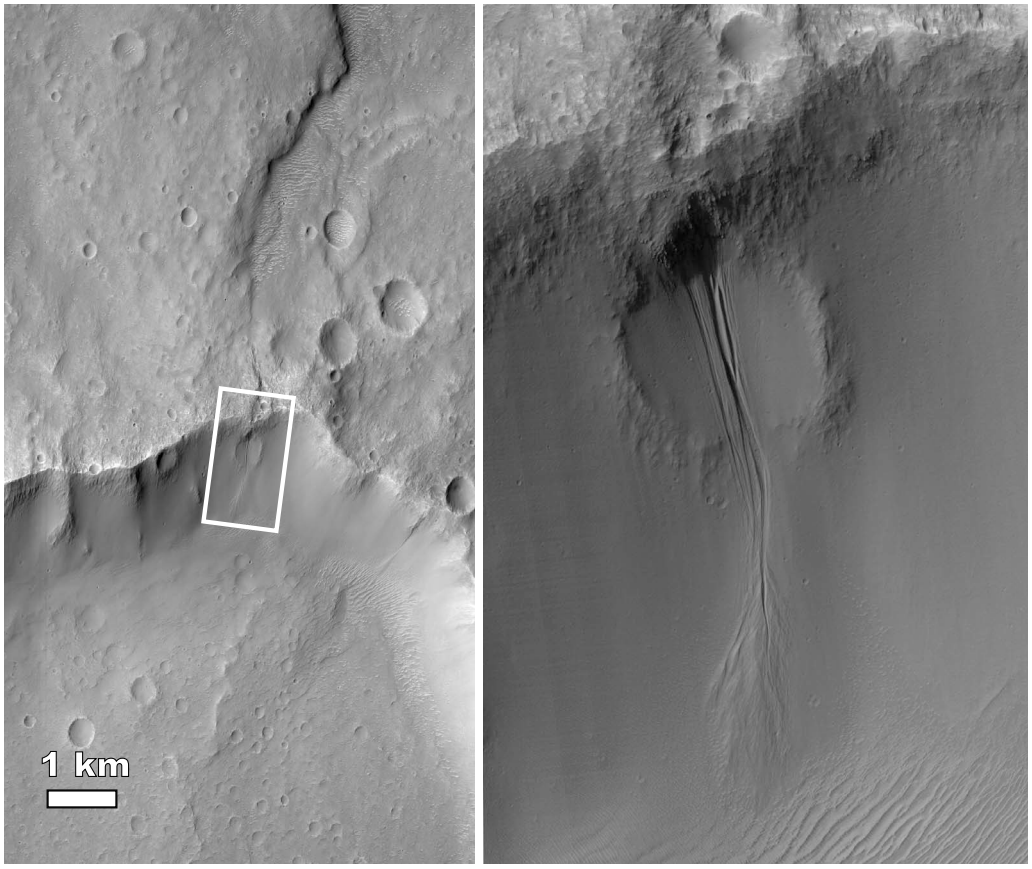


**Figure 15.** HiRISE image PSP_002068_1510 of the crater-fault intersection (left) and a close up view (right) of the gully. A small alcove is present at the exact intersection point.

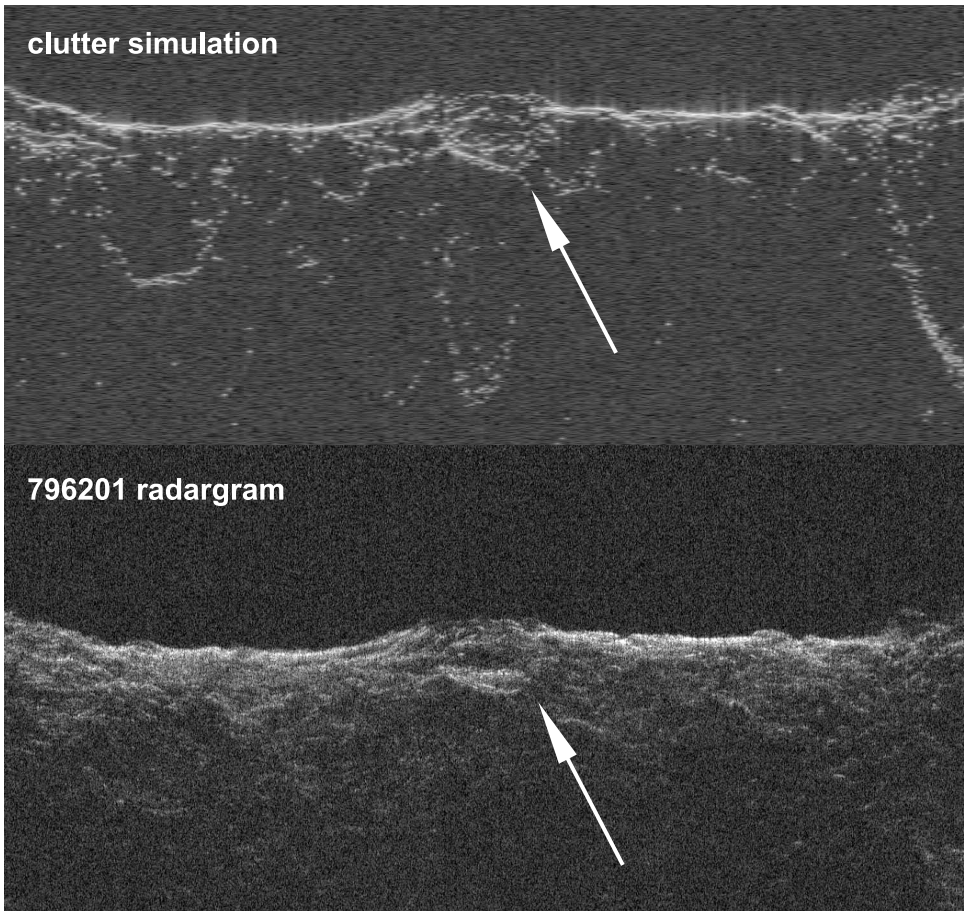


**Figure 16.** Radargram and simulated clutter for SHARAD track 796201, which transect the crater exactly over the area seen in Figure 14. The white arrow shows the location of the crater. Features in the radargram occurring later than the surface reflection can also be seen in the simulation, which identifies them as clutter. No consistent subsurface reflector is seen across the scene.

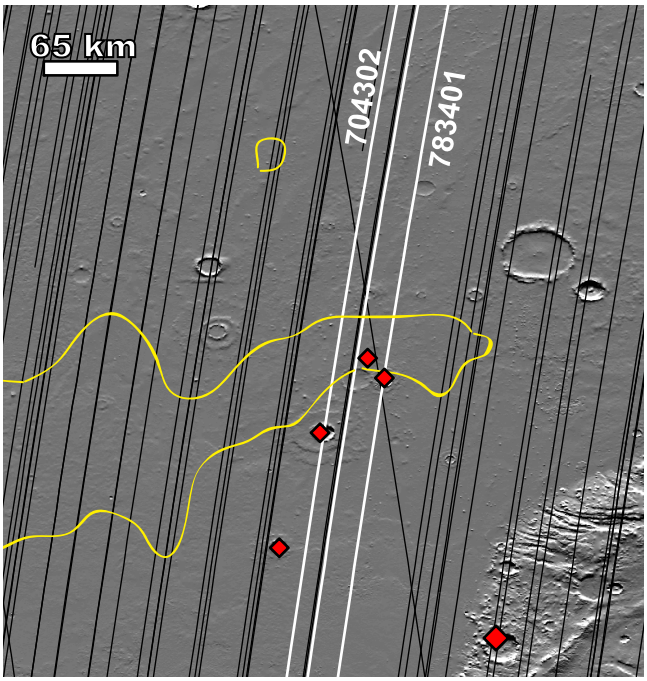


**Figure 17.** MOLA DEM covering the southeastern portion of Arcadia Planitia, with Lycus Sulci in the lower right. Diamonds denote gully locations, SHARAD tracks are shown as black lines, and tracks 704302 and 783401 are highlighted in white. Yellow contours correspond to the radar subsurface unit of *Plaut et al.* [2009a].

[2008], tailored towards martian compositions and radar sounder frequencies, show that the loss tangent $\tan\delta = \varepsilon''/\varepsilon'$ is roughly $10^{-1}$ or lower for expected regolith compositions (plagioclase, olivine, JSCM1) at soil-like densities (1.6 g cm$^{-3}$) and weakly dependent or independent of temperature and frequency. Gray hematite and magnetite have higher loss tangents, producing attenuation rates (dB m$^{-1}$) at least one order of magnitude higher than the lossiest of the silicic compositions. Here we take the imaginary portion of the permittivity of the overburden layer ($\varepsilon''_{ov}$) as a free-parameter, aiming to estimate the necessary value to suppress subsurface reflections from different aquifer scenarios.

[26] The presence of water in rocks and soils is another factor that can affect $\varepsilon$ greatly. The dielectric behavior of pure liquid water is described by the Debye equation, which depends on temperature and radar frequency [*Ulaby et al.*,

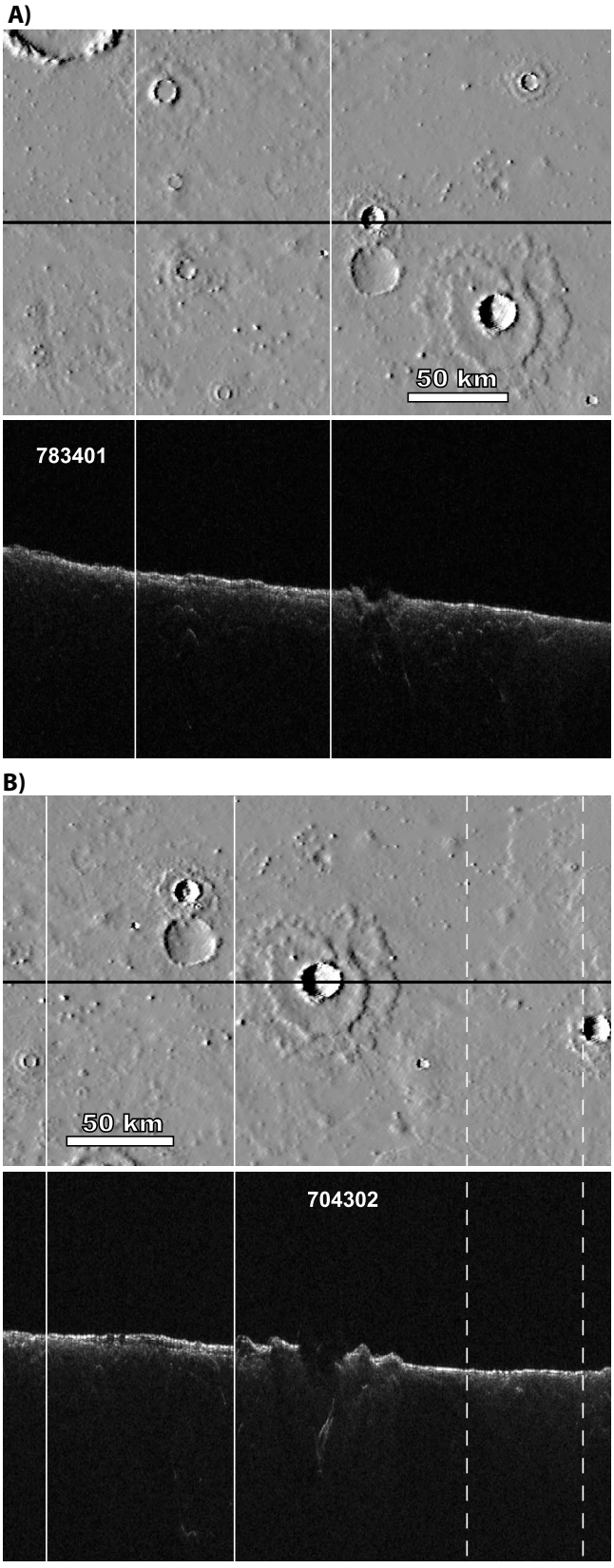


**Figure 18.** (a) Portion of SHARAD track 783401 (black line on DEM at the top) that intersects a gully-bearing crater in eastern Arcadia Planitia (41.46°N, 215.85°E) and the accompanying radargram. The crater is seen at the center of the radargram, while a subsurface reflector near parallel to the surface (bound by vertical white lines) is seen to the north (left) of it. Other returns following the surface reflection correspond to clutter. (b) Portion of SHARAD track 704302 (black line on DEM at the top) that intersects another gully-bearing crater in eastern Arcadia Planitia (40.35°N, 214.6°E) and the accompanying radargram. The crater is seen at the center of the radargram, while a subsurface reflector near parallel to the surface (bound by vertical white lines) is seen to the north (left) of it. To the south of the crater there appears to be a weak (near noise level) and deeper reflector (bound by vertical dashed white lines).

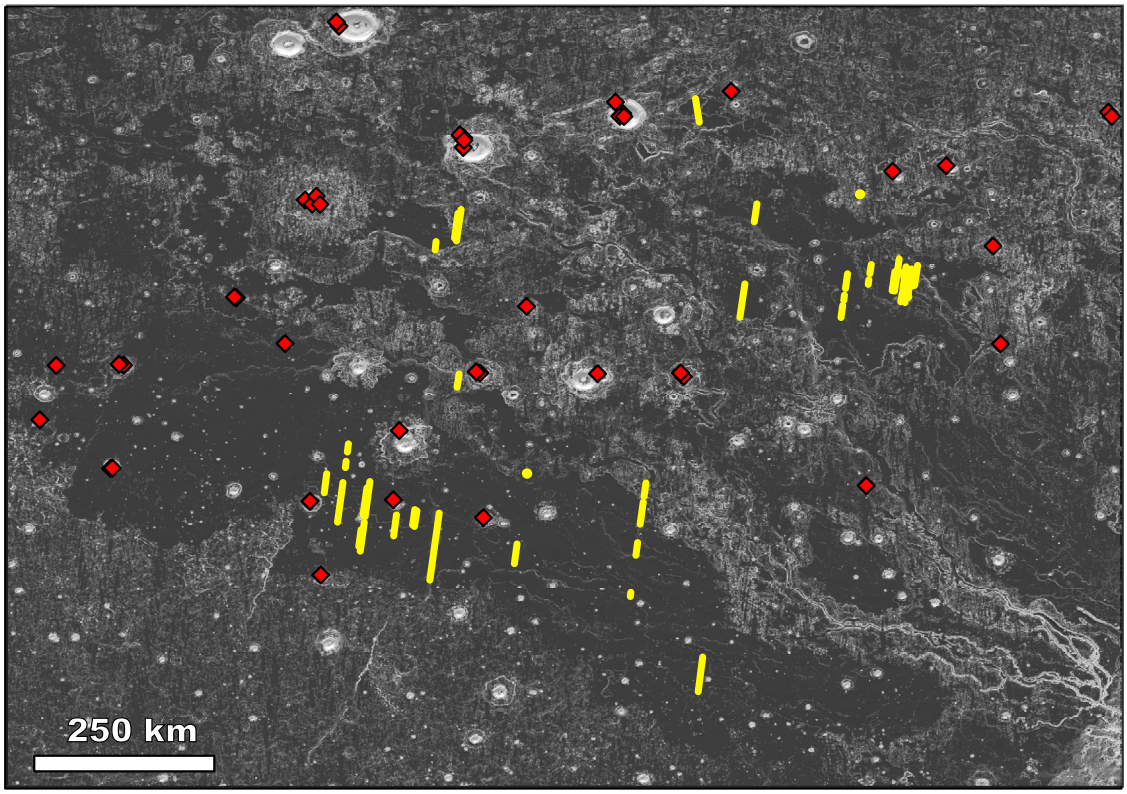


**Figure 19.** Composite of MOLA 128 pixel/degree shaded relief and roughness of southeastern Utopia Planitia, where a large number of craters host gullies (red diamonds). Grayscale corresponds to roughness, where smooth is dark and rough is bright. The lower slopes of Elysium Montes are in the lower right. Line segments in yellow correspond to portions of SHARAD tracks where a radar subsurface reflector has been detected.

1986]. Considering near freezing temperatures and 10 MHz frequency, the Debye equation yields $\varepsilon'_w = 84$. While $\varepsilon''_w$ of pure water is relatively low, adding salinity can boost it by several orders of magnitude, making the briny mixture much lossier. Because here we are concerned with the reflection produced by the upper surface of the aquifer, which depends on the contrast in the real portion of permittivity, we do not consider the control of salinity on $\varepsilon''_w$ and on the attenuation of the signal through aquifer. There are several models that can be used in such a calculation of the effective permittivity $\varepsilon_{mix}$ of a water-rock mix, depending on proportions of host to inclusions and inclusion shapes [e.g., *Nunes and Phillips*, 2006; *Ulaby et al.*, 1986], but the variational model of *Hashin and Shtrikman* [1962] for multiphase materials can be used to determine the upper and lower bounds of $\varepsilon_{mix}$ (or magnetic permeabilities, $\mu_{mix}$). Figure 22 shows the resulting upper and lower bounds for $\varepsilon'_{mix}$, using $\varepsilon'_w = 84$ and $\varepsilon'_{rx} = 5$, for up to 50% of water by volume (or saturated porosity). At low porosities, lower than 0.02%, $\varepsilon'_{mix} \sim 5$, while at a porosity of 50% the maximum possible value is $\varepsilon'_{mix} \sim 37$.

[27] To incorporate the well-defined upper bound to $\varepsilon'_{mix}$ as a function of porosity into the stratigraphic model of an overburden layer over an aquifer, we apply the propagation model of *Nunes and Phillips* [2006] for aquifer depths between 50 and 200 m (consistent with observed alcove depths) and $\varepsilon'_{ov}$ values between $10^{-3}$ and 1. Results from the simulations can be seen in Figure 23, which shows the expected aquifer reflection power normalized to the power of the surface reflection. The next question is then the power threshold necessary for a subsurface reflection. The average signal-to-noise ratio (SNR) can be estimated from SHARAD observations according to geologic setting by laterally averaging each vertical line (or record) in a radargram over a desired area, such as in Figure 7 for Gamboa crater. The power level preceding the surface reflection in all three cases in Figure 7 is ~1.75 ± 0.25 dB (one standard deviation) and is a good estimate for the galactic noise. In the case of smooth northern plains (Acidalia Planitia, in this example), the average power of the surface reflection is 45 ± 20 dB; the large uncertainty arises in the averaging process from both variations in power and slight variations in range due to a gently undulating surface. The average SNR is then the difference between the surface reflection power and the galactic noise, or ~43 dB. In rougher plains units, the average SNR drops to ~33 dB. Of course, variations in noise depend on other parameters, such the location of the spacecraft with respect to Sun because of ionospheric effects. In any case, the range in SNR is taken as representative of what is found for most of the radargrams examined.

[28] For all depths and aquifer porosities and considering the estimated range in SNR, the aquifer reflection lies above the signal-to-noise floor of the SHARAD system as long as $\varepsilon''_{ov} \leq 5 \times 10^{-2}$. A water rich aquifer with 50% porosity

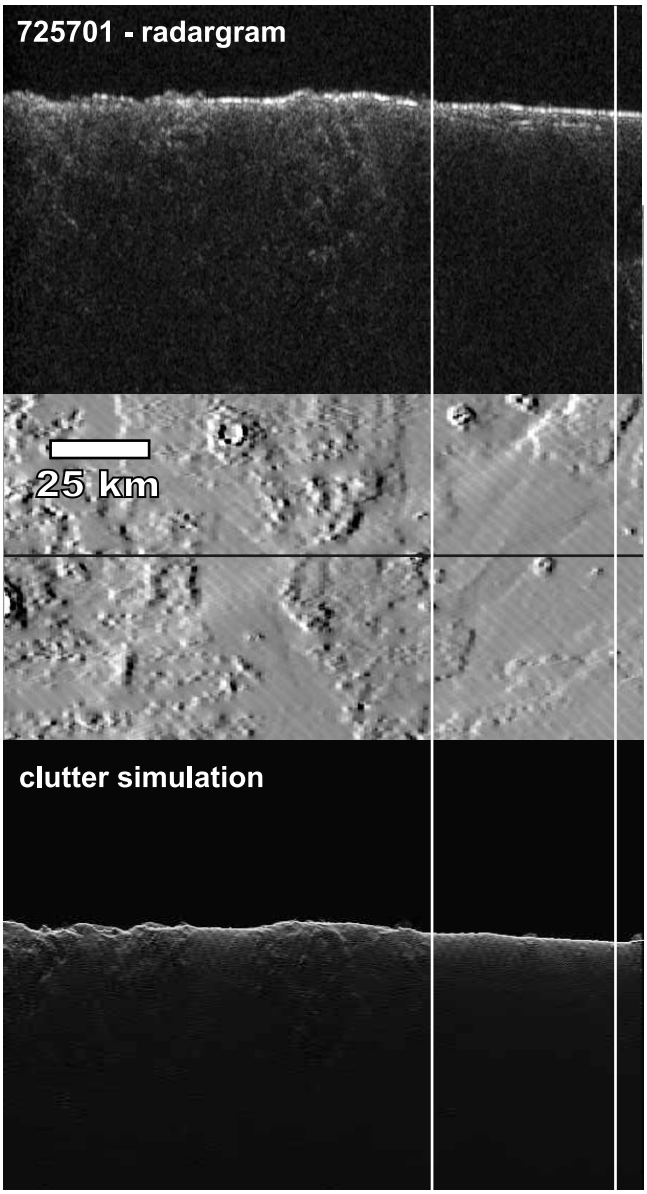


**Figure 20.** SHARAD ground track 725701 (center) and the accompanying radargram (top) and clutter simulation (bottom). A subsurface reflector, bound by vertical magenta lines, is present on the southern (right) portion of the radargram and correlates with the smoother surface as seen in the DEM. This reflector is absent from the surface clutter simulation, as expected. A gully-bearing crater is just beyond the north end of the track.

would be detectable at all of the adopted depths except in the case of $\varepsilon''_{ov} > 3 \times 10^{-1}$. Conversely, an aquifer that is poor in water due to a porosity value of only 1% could only be detected at the 50 to 200 meters depth range if $\varepsilon''_{ov} \leq 5 \times 10^{-2}$.

## 5. Discussion

[29] The majority of the gully sites we have examined with SHARAD show no indication of having associated subsurface reflectors. In general, sites in southern highlands have substantially more clutter than those in the northern lowlands, reflecting the rougher topography in the south and frequently necessitating clutter simulations for radargram interpretation. In select cases with ample SHARAD coverage,

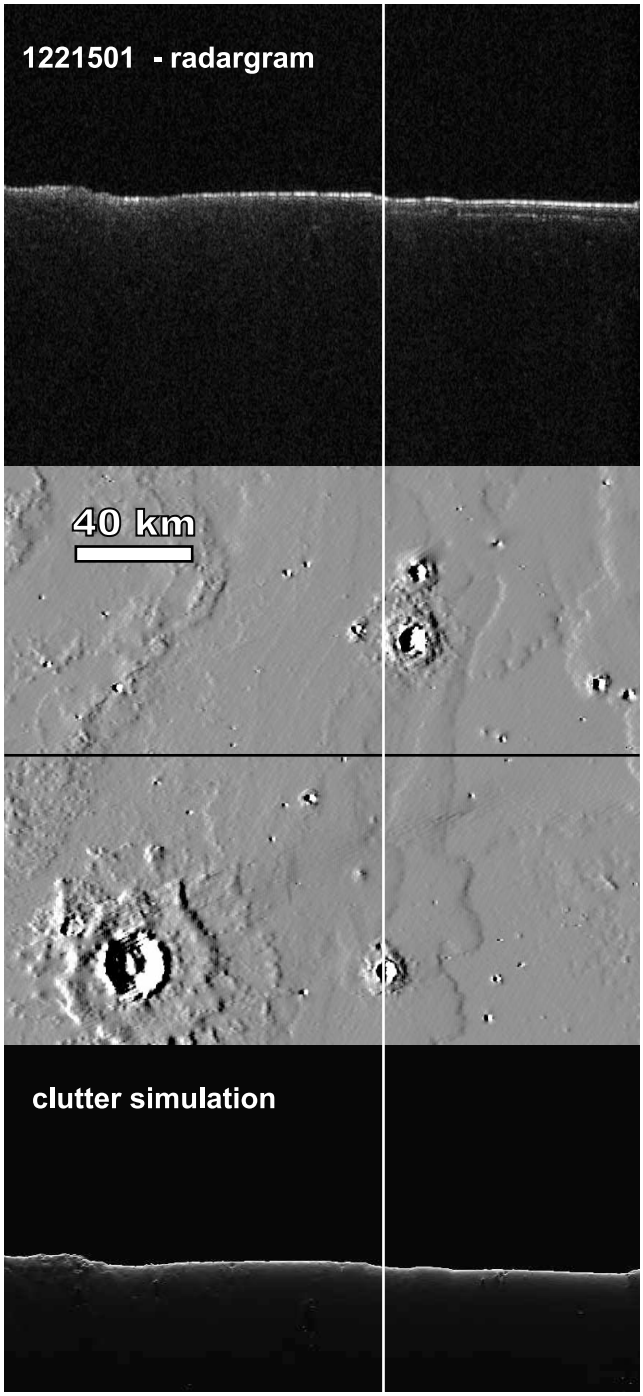


**Figure 21.** Portion of SHARAD ground track 1221501 and the accompanying radargram. A subsurface reflector, near parallel to the surface reflection is seen on the south (right) portion of the radargram. Its northern extremity is marked by the vertical white line and does not apparent correlate with surface relief. This track intersects the thick ejecta blanket of a gully-bearing crater near the north of the reflector (not shown).

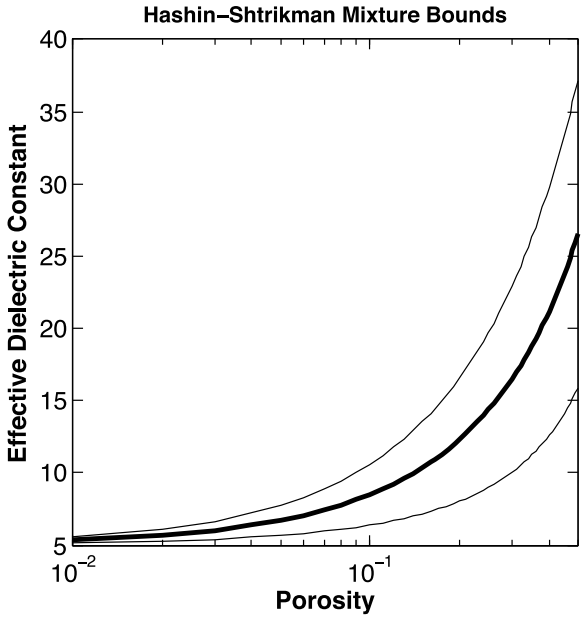


**Figure 22.** Theoretical limits (thin lines) for the effective real dielectric constant of a mixture of rock and pure liquid water according to the Hashin-Shtrikman model. The bold line corresponds to the mid-point between the upper and lower limits. The mixture proportions are a function of porosity and the assumption that pore space is saturated. For the case illustrated, $\varepsilon'_{rx} = 5$ and $\varepsilon'_{w} = 84$.

a simple comparison between two closely spaced radargrams provided guidance in determining clutter, as the lateral offset between tracks cause the clutter feature to change in shape and position from one radargram to the other. In areas of relatively smooth surface, sidelobes are prevalent and imitate in shape and power variations the strong surface reflection. In some cases where sidelobes persist despite using different signal processing approaches, albeit at a near-noise level, there is a possibility that a layer ~0.3 $\mu$s after and ~40 dB weaker than the surface reflection exists. In these cases the depth of the reflector is shallower than the depth from the local surface where gullies originate on their hosting slopes.

[30] Examination of certain gully sites with high likelihood for a ground water origin, such as the faulted crater in Terra Cimmeria, or presenting ongoing activity, such as the active gullies of *Malin et al.* [2006], revealed no subsurface reflectors. This result obviously weakens the aquifer hypothesis for gully formation, as these were some of the most promising sites for the detection of liquid water. However, it does not necessarily disprove the hypothesis. As the propagation models show, small amounts of water (1% or lower) can go undetected if the imaginary portion of the dielectric constant of the overburden layer is high (~$10^{-1}$ or higher). Such values are more compatible with materials containing electrically conductive or magnetic minerals (e.g., gray magnetite [*Stillman and Olhoeft*, 2008]), aqueous alteration minerals (e.g., phyllosilicates [*Grimm and Stillman*, 2008]), or adsorbed water [*Olhoeft et al.*, 1975]. These minerals in question are not known to occur everywhere on the surface of Mars based on other remote sensing techniques [e.g., *Christensen et al.*, 2001; *Poulet et al.*, 2005]. At the Phoenix landing site on the northern plains the Thermal and Electrical Conductivity Probe (TECP) measurements are consistent with an effective lack of charge transport in the shallow regolith [*Smith et al.*, 2009], which is a surprising find if water adsorption is to be widespread on Mars.

[31] Other possible effects beyond composition may contribute to radar attenuation in the Martian subsurface. Our propagation models only include smooth interfaces and uniform layers, so it is plausible that the contribution from surface (as seen in Figure 7) and volume scattering (as perhaps expected in heavily cratered terrains) in the overburden, and scattering at an upper aquifer boundary that is rough, may contribute to the suppression of subsurface reflections. In any case, it is not likely that shallow (~200 m) aquifers holding large amounts (10% to 50%) of liquid water would go undetected by SHARAD everywhere, as they would produce subsurface reflections with power possibly similar to that of surface reflections, depending on $\varepsilon''_{ov}$ and the smoothness of the aquifer interface. This assertion is strengthened by two other observations. One is the lack of subsurface reflectors resembling aquifers in observations made by the MARSIS radar sounder on board Mars Express [*Farrell et al.*, 2009], and the other is the revised Martian heat flux from 30 mW $m^{-2}$ to ~ 25 mW $m^{-2}$ as a consequence to the lack of lithospheric deflection beneath the load of the north polar cap as determined by SHARAD [*Phillips et al.*, 2008]. A lower heat flow likely causes a much thicker cryosphere and pushes the level of possible liquid ground water deeper into the crust.

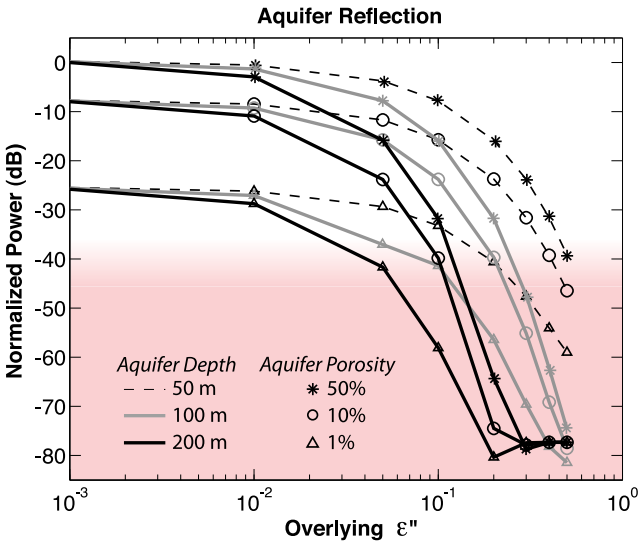


**Figure 23.** Results from a series of propagation models assuming a stratigraphy of an overburden overlying a saturated layer (aquifer). Shown is the expected strength of the reflection produced by the interface between the overburden and the aquifer for a series of aquifer (saturated) porosity values and imaginary dielectric constant for the overburden. Shaded area of the graph corresponds approximately to the regime below the measured signal-to-noise floor of SHARAD.

[32] The only two locations we have found, thus far, to possess subsurface reflectors in conjunction with gullies are those in eastern Arcadia and southeaster Utopia Planitiae. In both cases the reflectors are within 1$\mu$s from the surface reflection, which puts them in a depth range of 45 m to 90 m, assuming an effective permittivity for the overburden between 3 and 10. Such depths are compatible with the depths of no more than a few hundred meters to alcoves or gullies found by [*Malin and Edgett*, 2000]. Some of these reflectors seem to merge with the surface reflection at some points, as in Figure 18, which would be unlikely in the case of a shallow aquifer and is more consistent with the presence of ice in the subsurface, be it due to vapor diffusion, past depositional events, or other processes. Based on the geomorphology of surface features (flow features, fill deposits, mantling deposits, etc) and on the radar properties of the reflectors, *Plaut et al.* [2009a] also interpreted the radar unit in the volcanic plains of Arcadia Planitia to contain a large fraction of water ice. Here we also found similar reflectors in Utopia Planitia, which is also recognized as volcanic plains with some hydrovolcanic history interpreted as mega-lahars [*Russell and Head*, 2003]. As such, we preliminarily favor the interpretation of the Utopia reflectors as the signature of ice-rich layer near or at the surface.

[33] It is difficult to explain the origin of gullies based on SHARAD data alone, as only a few locations rich in gullies present subsurface radar signatures. In the cases that such signatures are present, the properties of the subsurface reflections in conjunction with surface geology, suggest ground ice over ground water. One important caveat to bear in mind is that we have not yet examined every possible gully location with SHARAD; it is possible that we may yet find locations where subsurface reflectors can be best interpreted as arising from ground water. Still, the best two sites where a relationship may exist between an observed subsurface reflector and gully sites is more favorable to mantling or ground ice sources. The targeting of gully sites is still ongoing and the analysis of the bountiful SHARAD (~12 TB at the time of this writing and growing) dataset is still in its infancy, and a more extensive analysis is due.

[34] **Acknowledgments.** This work is dedicated to the memory of our colleague and friend Ali Safaeinili, who was a superb radar scientist and a true gentleman. The authors would like to recognize the efforts of the entire SHARAD team in operating the instruments and in various scientific discussions. DCN would like to thank the support from the Mars Reconnaissance Orbiter project, Jennifer Heldmann and Nathan Bridges for sharing their gully databases, and Jeff Plaut for his comments. The manuscript benefited from the constructive input from two anonymous reviewers. This research was carried out at the Jet Propulsion Laboratory, California Institute of Technology, under a contract with the National Aeronautics and Space Administration.

## References

Allen, C. C., et al. (1997), JSC Mars-1: Mars regolith simulant, 28*th Lunar Planet. Sci. Conf.*, 1797, Houston, TX.

Balme, M., et al. (2006), Orientation and distribution of recent gullies in the southern hemisphere of Mars: Observations from High Resolution Stereo Camera/Mars Express (HRSC/MEX) and Mars Orbiter Camera/Mars Global Surveyor (MOC/MGS) data, *J. Geophys. Res.*, *111*(E5), E05001, doi:10.1029/2005JE002607.

Bibring, J.-P., et al. (2004), Perennial water ice identified in the south polar cap of Mars, *Nature*, *428*, 627–630.

Boynton, W. V., et al. (2002), Distribution of hydrogen in the near surface of Mars: Evidence for subsurface ice deposits, *Science*, *297*, 81–85.

Carr, M. H. (1979), Formation of Martian flood features by release of water from confined aquifers, *J. Geophys. Res.*, *84*(B6), 2995–3007.

Carr, M. H., and G. D. Clow (1981), Martian channels and valleys: Their characteristics, distribution, and age, *Icarus*, *48*(1), 91–117.

Christensen, P. R. (2003), Formation of recent martian gullies through melting of extensive water-rich snow deposits, *Nature*, *422*, 45–48.

Christensen, P. R., et al. (2001), Mars Global Surveyor Thermal Emission Spectrometer experiment: Investigation description and surface science results, *J. Geophy. Res.*, *106* (E10), 23,823–23,871.

Clifford, S. M. (1987), Polar basal melting on Mars, *J. Geophys. Res.*, *92*(B9), 9135–9152.

Clifford, S. M., and T. J. Parker (2001), The evolution of the Martian hydrosphere: Implications for the fate of a primordial ocean and the current state of the northern plains, *Icarus*, *154*(1), 40–79.

Costard, F., et al. (2002), Formation of recent Martian debris flows by melting of near surface ground ice at high obliquity, *Science*, *295*, 110–113.

Dickson, J. L., and J. W. Head (2009), The formation and evolution of youthful gullies on Mars: Gullies as the late-stage phase of Mars' most recent ice age, *Icarus*, *204*(1), 63–86.

Ducoff, M. R., and B. W. Tietjen (2008), Pulse compression radar, in *Radar Handbook*, edited by M. I. Skolnik, pp. 8.1–8.44, McGraw Hill, New York, NY.

Farrell, W. M., et al. (2009), Is the Martian water table hidden from radar view?, *Geophys. Res. Lett.*, *36*(15), L15206, doi:10.1029/2009GL038945.

Feldman, W. C., et al. (2002), Global distribution of neutrons from Mars: results from Mars Odyssey, *Science*, *297*, 75–78.

Grimm, R. E., and D. E. Stillman (2008), On the origin of widespread subsurface radar attenuation at Mars, in *39th Lunar Planet. Sci. Conf.*, 2251, Lunar and Planetary Institute, League City, TX.

Hanna, J. C., and R. J. Phillips (2005), Hydrological modeling of the Martian crust with application to the pressurization of aquifers, *J. Geophys. Res.*, *110*(E1) E01004, doi:10.1029/2004JE002330.

Hashin, Z., and S. Shtrikman (1962), A variational approach to the theory of the effective magnetic permeability of multiphase materials, *J. Applied Phys.*, *33*(10), 3125–3131.

Head, J. W., et al. (2008), Formation of gullies on Mars: Link to recent climate history and insolation microenvironments implicate surface water flow origin, *Proc. Natl. Acad. Sci.*, *105*(36), 13,258–13,263.

Heldmann, J. L., and M. T. Mellon (2004), Observations of martian gullies and constraints on potential formation mechanisms, *Icarus*, *168*(2), 285–304.

Heldmann, J. L., et al. (2007), Observations of martian gullies and constraints on potential formation mechanisms: II. The northern hemisphere, *Icarus*, *188*(2), 324–344.

Holt, J. W., et al. (2008), Radar Sounding Evidence for Buried Glaciers in the Southern Mid-Latitudes of Mars, *Science*, *322*, 1235–1238.

Kolb, K. J., et al. (2009), Measuring slopes of gully fan apices using digital elevation models, in *40th Lunar Planet. Sci. Conf.*, 2268, Woodlands, TX.

Malin, M. C., and K. S. Edgett (2000), Evidence for recent groundwater seepage and surface runoff on Mars, *Science*, *288*, 2330–2335.

Malin, M. C., and K. S. Edgett (2001), Mars Global Surveyor Mars Orbiter Camera: Interplanetary cruise through primary mission, *J. Geophys. Res.*, *106*(E10), 23,429–23,570.

Malin, M. C., et al. (2006), Present-Day Impact Cratering Rate and Contemporary Gully Activity on Mars, *Science*, *314*(5805), 1573–1577.

McEwen, A. S., et al. (2007), A Closer Look at Water-Related Geologic Activity on Mars, *Science*, *317*, 1706–1709.

Mellon, M. T., and R. J. Phillips (2001), Recent gullies on Mars and the source of liquid water, *J. Geophys. Res.*, *106*(E10), 23,165–23,179.

Mellon, M. T., et al. (2008), A prelanding assessment of the ice table depth and ground ice characteristics in Martian permafrost at the Phoenix landing site, *J. Geophys. Res.*, *113*(E11), E00A25, doi:10.1029/2007JE003067.

Mustard, J. F., et al. (2008), Hydrated silicate minerals on Mars observed by the Mars Reconnaissance Orbiter CRISM instrument, *Nature*, *454*, 305–309.

Nunes, D. C., and R. J. Phillips (2006), Radar subsurface mapping of the polar layered deposits on Mars, *J. Geophys. Res.*, *111*(E6), E06S21, doi:10.1029/2005JE002609.

Olhoeft, G. R., and D. W. Strangway (1975), Dielectric properties of the first 100 meters of the Moon, *Earth Planet. Sci. Lett.*, *24*, 394–404.

Olhoeft, G. R., et al. (1975), Effects of water on electrical properties of lunar fines, *6th Lunar Sci. Conf.*, 3333–3342, Houston, TX.

Phillips, R. J., et al. (1973), The Apollo 17 Lunar Sounder, *4th Lunar Sci. Conf.*, 2821–2831, Houston, TX.

Phillips, R. J., et al. (2008), Mars North Polar Deposits: Stratigraphy, Age, and Geodynamical Response, *Science*, *320*(5880), 1182–1185.

Picardi, G., et al. (2005), Radar sounding of the subsurface of Mars, *Science*, *310*, 1925–1928.

Plaut, J. J., et al. (2009a), A widespread radar-transparent layer detected by SHARAD in Arcadia Planitia, Mars, *40th Lunar Planet. Sci. Conf.*, 2312, Houston, TX.

Plaut, J. J., et al. (2009b), Radar evidence for ice in lobate debris aprons in the mid-northern latitudes of Mars, *Geophys. Res. Lett.*, *36*(2), L02203, doi:10.1029/2008GL036379.

Poulet, F., et al. (2005), Phyllosilicates on Mars and implications for early martian climate, *Nature*, *438*(7068), 623–627.

Russell, P. S., and J. W. Head (2003), Elysium-Utopia flows as megalahars: A model of dike intrusion, cryosphere cracking, and water-sediment release, *J. Geophys. Res.*, *108*(E6), 5064, doi:10.1029/2002JE001995.

Schon, S. C., et al. (2009), Unique chronostratigraphic marker in depositional fan stratigraphy on Mars: Evidence for ca. 1.25 Ma gully activity and surficial meltwater origin, *Geology*, *37*, 207–210.

Seu, R., et al. (2004), SHARAD: The MRO 2005 shallow radar, *Planet. Space Sci.*, *52*, 157–166, doi:110.1016/j.pss.2003.1008.1024.

Seu, R., et al. (2007), SHARAD sounding radar on the Mars Reconnaissance Orbiter, *J. Geophys. Res.*, *112*(E5), E05S05, doi:10.1029/2006JE002745.

Sharp, R. P., and M. C. Malin (1975), Channels on Mars, *Geol. Soc. Am. Bull.*, *86*(5), 593–609.

Skinner, J. J. A., et al. (2006), Digital renovation of the Atlas of Mars 1:15,000,000-scale global geologic series maps, *37th Lunar Planet. Sci. Conf.*, 2331, Houston, TX.

Smith, P. H., et al. (2009), $H_2O$ at the Phoenix Landing Site, *Science*, *325*(5936), 58–61.

Squyres, S. W., et al. (2006), Overview of the Opportunity Mars Exploration Rover Mission to Meridiani Planum: Eagle Crater to Purgatory Ripple, *J. Geophys. Res.*, *111*(E12), E12S12, doi:10.1029/2006JE002771.

Stillman, D., and G. Olhoeft (2008), Frequency and temperature dependence in electromagnetic properties of Martian analog minerals, *J. Geophys. Res.*, *113*(E9), E09005, doi:10.1029/2007JE002977.

Treiman, A. H. (2003), Geologic settings of Martian gullies: Implications for their origins, *J. Geophys. Res.*, *108*(E4), 8031, doi:10.1029/2002JE001900.

Ulaby, F. T., et al. (1986), *Microwave Remote Sensing: Active and Passive*, Artech House, Norwood, MA.

Wait, J. R. (1970), *Electromagnetic waves on stratified media*, 2nd ed., Pergamon Press, New York, NY.

B. Campbell, Center for Earth and Planetary Studies, Smithsonian Institution, Independence Ave., SW, Washington, DC 20013-7012, USA.

J. Holt, Department of Geological Sciences, University of Texas at Austin, 1 University Station, C1160, Austin, TX 78712-0254, USA.

D. C. Nunes, Jet Propulsion Laboratory, California Institute of Technology, 4800 Oak Grove Dr., MS 183-301, Pasadena, CA 91101, USA. (Daniel.Nunes@jpl.nasa.gov)

R. J. Phillips, Planetary Sciences, Southwest Research Institute, 1050 Walnut St., Boulder, CO 80302, USA.

R. Seu, Dipartimento INFOCOM, Università di Roma "La Sapienza," I-00184 Rome, Italy.

S. E. Smrekar, Earth and Space Science, Jet Propulsion Laboratory, California Institute of Technology, 4800 Oak Grove Dr., Pasadena, CA 91101, USA.